Journal of Energy Storage 53 (2022) 105140

Contents lists available at ScienceDirect

Journal of Energy Storage

journal homepage: www.elsevier.com/locate/est

Review article

An overview on the use of additives and preparation procedure in phase change materials for thermal energy storage with a focus on long term applications

Alessandro Ribezzo, Gabriele Falciani, Luca Bergamasco, Matteo Fasano, Eliodoro Chiavazzo *

Department of Energy, Politecnico di Torino, Corso Duca degli Abruzzi 24, 10129 Torino, Italy

ARTICLE INFO

Keywords:
Thermal energy storage
Phase change materials
Additives
Thermal conductivity
Long term heat storage

ABSTRACT

In this review we aim at providing an up-to-date and comprehensive overview on the use of additives within selected Phase Change Materials (PCMs) from both an experimental and more theoretical perspective. Traditionally, mostly focusing on short-term thermal energy storage applications, the addition of (nano)fillers has been extensively studied to enhance unsatisfactory thermo-physical properties in PCMs, in order to overcome limiting aspects such as low thermal conductivity possibly leading to unacceptable long charging and/or discharging periods and inefficient heat-storage systems. On the other hand, here we focus on the most important PCMs for long-term thermal energy storage (i.e. spanning from classical solid-to-liquid to more recent solid-to-solid PCMs) and make an effort in shedding light on the role played not only by additives but also (and importantly) by additivation protocols on the resulting thermo-physical and stability properties. While introducing and connecting to general advantages related to additivation in classical PCMs for thermal energy storage, we discuss specifically the use of additives in sugar alcohols and sodium acetate trihydrate, as well as in novel emerging classes of PCMs capable of undergoing solid-to-solid transitions and showing promising features for long-term heat storage materials. We highlight outstanding issues in the use of additives for property enhancement in PCMs and expect that the present work can contribute to expand the current understanding and field of application of the less mature PCMs for thermal energy storage, especially as far as long term applications are concerned.

1. Introduction

Thermal energy storage (TES) technologies are essential for the exploitation of intermittent renewable source of energies, as they can decouple the power generation and supply availability [1–3]. According to the 2020 Innovation Outlook on Thermal Energy Storage by the International Energy Agency, the TES global market could triple in size by 2030—rising from 234 GWh of installed capacity in 2019 to over 800 GWh within the upcoming decade [4].

TESs can be classified in chemical storage, in which reversible chemical reactions are exploited [5–9], and physical storage, that is divided into sensible and latent heat storage. Sensible heat storage accumulates heat by exploiting the heat capacities of materials; in this case, the amount of stored heat depends on the temperature gradient, mass, and specific heat capacity of the material [10]. Latent heat storage materials, instead, generally referred to as Phase Change Materials (PCMs), exploit a phase transition to store and release thermal energy at constant temperature, thereby exhibiting a higher heat storage density and a narrower temperature change as compared to sensible storage methods [11]. The total quantity of the heat stored by a PCM over the temperature interval of the process is the summation of the latent and sensible heat [12].

PCMs are progressively evolving from the lab to the application scale in various fields such as solar energy storage [13–15], waste heat recovery [16], buildings [17,18], clothing [19,20], thermal protection systems, and electronics [21].

In PCMs, solid-to-gas and liquid-to-gas phase transitions are typically avoided, owing to the large variations in their volume. Solid-to-solid phase transition occurs between two solid phases, and these materials deliver relatively low enthalpies of solid transition (i.e., lower than 100 kJ/kg) that are characterized by reduced volume variations and ease of containment [22]. Solid-to-liquid transitions are the most prevalent in PCM applications, and they exhibit high enthalpy variations (between 100 and 300 kJ/kg [23]) with relatively small volume variations during the phase transition (<10%).

* Corresponding author.
E-mail address: eliodoro.chiavazzo@polito.it (E. Chiavazzo).

https://doi.org/10.1016/j.est.2022.105140
Received 21 January 2022; Received in revised form 29 April 2022; Accepted 14 June 2022
Available online 28 June 2022

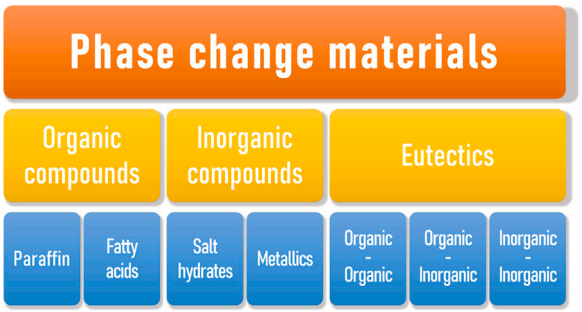

Fig. 1. Classification of PCMs according to their nature.

The essential properties of a PCM required for storage application include the transition temperature and latent heat. The latent heat has to be adequately large to achieve high energy storage densities. Moreover, a transition temperature between the charging (melting) and discharging (solidification) temperatures is required to exploit the entire latent heat of the PCM. In particular, PCMs can be classified based on their transition temperature as subambient (–33 to 27 °C), ambient (21 to 28 °C), moderate (40 to 100 °C) and high-temperature (several hundreds to over 1000 °C) ones [10]. In addition, certain other properties of critical importance for a PCM include density, thermal conductivity, stability, cyclability, presence of subcooling, cost and safety of use. Thermal conductivity is one of the major bottlenecks for the applications of PCMs. Owing to its generally reduced value (0.2–0.8 W/m K), the charging and discharging processes may be slow, and thus, their power density lower than other TES technologies. Furthermore, longer charging/discharging periods may result in incomplete melting/solidification processes, and therefore, enable only a partial exploitation of the maximum storable energy [24]. In particular, thermal, physical, and chemical properties should not exhibit a significant reduction during cycles. A major limitation of the cyclability is represented by the irreversible separation into various phases, which is typical for PCMs containing more than a single component.

As depicted in Fig. 1, PCMs can be classified according to their nature, namely, organic compounds (paraffins or fatty acids [25]), inorganic compounds (salt hydrates or metallics), and eutectic mixtures.

The applications of PCMs can be categorized into short- [26] and long-term heat storage [27]. In the former, the PCM cools down and attains its phase transition temperature then releasing the latent heat. In long-term applications, the latent thermal energy can be stored for a longer period (weeks or months), even if the temperature is less than the transition temperature of the specific PCM. This can be achieved exploiting the subcooling phenomena, which is typical among most PCMs. In context, subcooling is defined as the difference between the temperature of phase changes during the heating and cooling processes. Although subcooling is undesired and thus avoided in short-term applications to maintain a constant phase-change temperature during heat charging/discharging applications, it is essential for long-term applications. Under subcooling conditions, the PCM remains in a metastable equilibrium state, if it is not triggered from an external source such as ultrasound waves [28], materials addition [29], and mechanical stress [30,31]. Subsequently, the stored latent heat is released after the system is triggered [32].

In the context of long-term energy storage, solid-to-solid PCMs are recently garnering considerable attention owing to the discovery of materials, mainly plastic crystals, with high enthalpy of transition between the solid phases [33]. They avoid the liquid phase and offer several advantages in comparison to the solid-to-liquid PCMs, such as lack of leakages and of precipitation in heterogeneous mixtures.

Certain issues are limiting the development of PCMs for long-term storage applications, i.e., their low thermal conductivity, poor cyclability, and phase-transition temperatures, which are inadequate for sub-ambient, ambient and moderate conditions. The low thermal conductivity of these materials, mostly paraffins and fatty acid, acts as the major limitation as it reduces the heat transfer inside the PCM [34], thereby increasing the charging and discharging periods and decreasing the storage efficiency. Furthermore, a majority of these materials presents poor cyclability owing to a rapid degradation of either the material or the properties of the container [35]. Ultimately, the unpredictable stability of supercooled systems requires more efforts to obtain stable TES systems for practical applications. Thus, we hereby review the use of addition of various elements inside a PCM matrix to surpass the above-mentioned limitations.

Several reviews on PCMs and their additivation are available in the existing literature; however, they are generally focused on specific applications (e.g. short-term applications [36,37], such as domestic heating [38], thermal management of batteries [39], or solar thermal storage [40]), on specific properties to be enhanced (e.g., thermal conductivity [41,42] or subcooling [43,44]) or on specific additives and PCMs (e.g. carbon-based nanofillers [45,46]). Here, we aim to provide a general and comprehensive overview of the major solutions for the application of additives in several fields related to the TES, i.e., from enhancing the thermal conductivity to the stabilization of the subcooling in PCMs for long-term applications. Moreover, we elucidate a comprehensive vision of the additivation topic based on the theoretical as well as the practical perspective. The additives and their influence on PCMs properties that are investigated in this review are summarized in Fig. 2 for an immediate overview.

The outline of this work is as follows. The different approaches used for obtaining thermal conductivity enhancement in PCMs are reviewed in Section 2. In particular, we focus on the additivation of nanofillers, comparing different fillers and experimental procedures. In Section 3, we discuss the two primary long-term PCMs, sodium acetate trihydrate and sugar alcohols, together with their relative eutectic mixtures and additivation. An overview of solid-to-solid PCMs and the effect of additives is presented in Section 4. Conclusions are finally drawn in Section 5.

2. Thermal conductivity enhancement

A major issue limiting large-scale applications of PCMs relates to their low thermal conductivities, which generally ranges 0.1–0.8 W/m K [41]. This implies slower response time and thus longer thermal charge/discharge processes, which may finally yield incomplete melting/solidification and lower storage densities [47]. In case of partial melting/solidification, latent TES may even be disadvantageous in practical applications as compared to sensible TES [24]. Consequently, several additivation methods have been proposed in the existing literature to enhance the thermal conductivity of PCMs.

2.1. Types of additives

One of the most popular approaches entails the combination of PCMs with highly conductive materials, thereby obtaining PCM composites [48]. For example, Sunxi et al. [49] introduced an octanoic-myristic acid binary eutectic mixture inside the porous structure of the expanded graphite to enhance the thermal conductivity of PCMs and increased the thermal conductivity by 2.36 times at 7% weight content of graphite. Al-Shannaq et al. [50,51] proposed the use of spherical composites developed from a conductive sphere of graphite-impregnated PCM (refer to Fig. 3) and obtained up to a 30-fold enhancement in its thermal conductivity. However, the above-mentioned methods posed a major limitation—a remarkable reduction in the latent heat of the composite—owing to the relatively high content of non-PCM material inside the composite.

Lately, nanotechnology-based solutions have been developed to achieve a more effective enhancement of the thermal conductivity without significantly modifying the base properties of the PCM. These

		PCM			
		Short term solid-liquid	Long term solid-liquid		Solid-solid
			SAT	SA	
PROPERTIES	Thermal conductivity	Carbon-based (GNP-CNT-CNF)	Water Graphite Thickeners	Graphite Metal based	GNP Graphite Metal based
	Latent heat	Carbon-based (GNP-CNT-CNF)	Water* Thickeners*	Water	GNP Graphite Metal based
	Subcooling**	Carbon-based (GNP-CNT-CNF)	Water Thickeners	Graphite	GNP Graphite Metal based
	Precipitation	Carbon-based (GNP-CNT-CNF)	Water Graphite Thickeners	---	---

Fig. 2. Summary of materials and properties reviewed in this work. Background colors refer to the impact of the additives on a specific property: green stands for a positive impact, red for a negative impact and gray for a negligible one. For example, for short term application solid–liquid PCM, CNTs improve the overall effective thermal conductivity (green color), reduce the latent heat (red color) and reduce the stability of the nanocomposite due to an increased precipitation (red color). *water and thickeners enhance the latent heat up to a specific content. **subcooling colors depend on the specific application considered. In short term applications, a positive impact (green color) denotes a reduction of the subcooling. In contrast, the green color indicates an increase of the subcooling in long term applications. (For interpretation of the references to color in this figure legend, the reader is referred to the web version of this article.)

Fig. 3. Images of a sample sphere during the production of the organic PCM composite. (a) Compacted sphere of graphite of 78 mm diameter; (b) impregnation of sphere with organic PCM; (c) coating of sphere with thin polymeric shell to avert leakages.
Source: Image sourced from Ref. [50].

Table 1
Main properties of interest (aspect ratio, thermal conductivity and dispersion) for the considered nanofillers, namely carbon nanotubes (CNT), carbon nanofibers (CNF) and graphene nanoplatelets (GNP).

Nanoadditive	Aspect ratio	Thermal conductivity	Dispersion
CNT	1250 ÷ 3750 [57]	2400 ÷ 4740 W/m K [54]	Poor [58]
CNF	~277 [58]	~ 1950 W/m K [58]	Good [58]
GNP	$\sim 10^3$ [59][a]	In-plane: 3000 ÷ 6500 W/m K, Out-of-plane: 6 W/m K [55]	Excellent [60]

[a]For CNTs and CNFs the aspect ratio is defined as the ratio between the length and the diameter of the filler, for GNPs the aspect ratio is diameter/length.

solutions involve the addition of highly conductive nanofillers inside the PCM matrix at low content, such as nanometals, nanometal oxides, and nanocarbons [52].

The most common nanostructures include carbon-based nanoparticles such as carbon nanotubes (CNTs) and graphene nanoplatelets (GNPs), owing to their outstanding mechanical and thermal properties combined with the reduced costs [53]. For example, pristine CNTs have thermal conductivity ranging from 2400 to 4740 W/m K [54]. Graphene nanoplatelets, which are characterized by a remarkable anisotropy, have an in-plane thermal conductivity of 3000 ÷ 6500 W/m K and an out-of-plane thermal conductivity of 6 W/m K [55]. The actual thermal conductivity of these carbon nanofillers generally depends on several properties as geometric (diameter, length, aspect ratio of nanofiller and overlap between nanofillers) and chemical aspects (number of covalent interlinks, functionalizations) [56]. As an overview, Table 1 provides a summary of the features of the carbon-based nanofillers reviewed in this section.

An important phenomenon for consideration in composites pertains to the thermal resistance at the interfaces between the filler particles and the base PCM. Such interfacial resistance may have several origins, including: (i) air inclusions caused by a non-perfect mechanical contact between the two phases, that generates a smaller effective contact area between the filler and matrix [61]; (ii) phonon scattering at the interface, owing to the spectra mismatch between filler and matrix [62]. These thermal resistances at the interface play an important role on the heat transport inside the composite, as they limit the enhancement of the overall effective thermal conductivity of the composite. Atomistic studies based on molecular dynamics simulations have become used for understanding thermal interface phenomena [56, 63–65]: these simulations can be useful for determining appropriate methods to limit the impact of interface resistances and completely exploit nanotechnologies-based composites [56].

The inclusion of nanofillers enhances the thermal conductivity of the various phases of the PCM, as reported in the studies of Kumaresan et al. [66], where multiwalled carbon-nanotubes (MWCNTs) are introduced in a paraffin-based matrix. As depicted in Fig. 4 (top), a rise in thermal conductivity was observed for both the solid and liquid phases. In detail, the effective thermal conductivity of the composite PCM attained a maximum value close to 0.4 W/m K (1.5-fold enhancement) for 0.6% weight content of filler at 20 °C (solid phase), followed by a reduction in the thermal conductivity values in the liquid phase (the melting temperature range was between 18 and 23 °C). The thermal conductivity enhancement (computed as λ_{eff}/λ_m, where λ_{eff} denotes the effective thermal conductivity of the nanocomposite and λ_m represents that of the pristine PCM) as a function of temperature for samples additivated with various MWCNTs weight contents is illustrated in Fig. 4 (bottom). A similar V-shape trend was observed for all the contents, wherein the minimum value locates in the temperature range of phase transition. This phenomenon can be attributed to the molecular disorder during the phase transitions, which hinders the enhancement generated by the additivation of MWCNTs [66]. In general, the introduction of fillers inside a PCM enhances the thermal conductivity in both the solid and liquid phases. Moreover, the increase

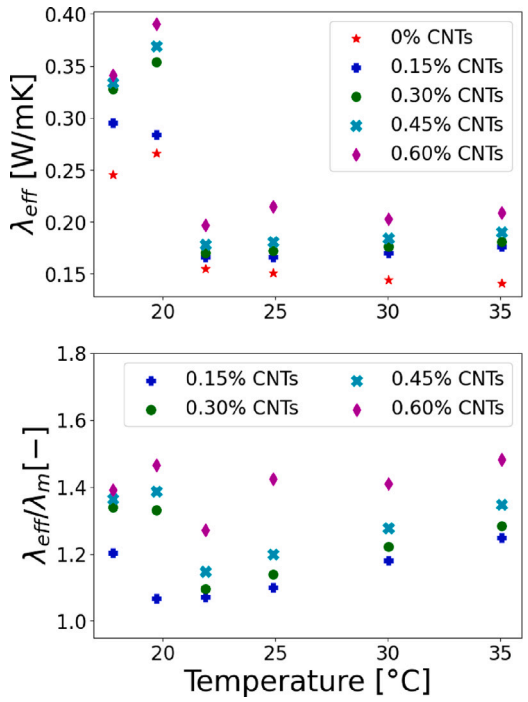

Fig. 4. Top: thermal conductivity of pure and additivated paraffin-based PCM as a function of temperature and weight content of fillers. Bottom: thermal conductivity enhancement of additivated PCM as a function of temperature and weight content of fillers. λ_{eff} is the effective thermal conductivity of the composite, λ_m is the thermal conductivity of the matrix alone [66].

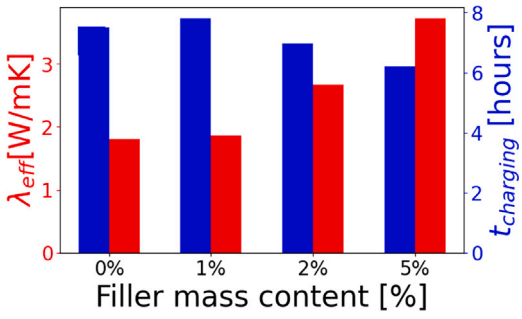

Fig. 5. Thermal conductivities and charging periods of pristine eutectic salt of $LiNO_3$–KCl based nanocomposite as a function of functionalized GNPs weight content. λ_{eff} is the effective thermal conductivity of the composite, $t_{charging}$ is the time needed to complete the melting of the PCM [67]. (For interpretation of the references to color in this figure legend, the reader is referred to the web version of this article.)

Table 2
Comparison between thermal conductivity enhancement and charging periods for a soy wax-based PCM additivated with CNFs and CNTs [58]. Notably, the term "charging period" is used to define the time interval that is required to attain a temperature of 36 °C from 24 °C, wherein the melting point of the soy wax is 54 °C.

Nanofiller	Weight content [%]	λ_{eff}/λ_m [−]	Reduction in charging periods [%]
CNFs	1	1.27	23
	2	1.32	38
	5	1.44	61
	10	1.45	71
CNTs	1	1.05	13.4
	2	1.09	23
	5	1.22	30
	10	1.24	26

in the thermal conductivity of composite PCMs decreases the cooling periods measured at the center of the cylindrical sample tested with a maximum value of 33.64% at 0.6% weight content of filler. Notably, an increase in the thermal conductivity by nanofiller additivation does not always reduces the charging/discharging periods.

Singh et al. [67] analyzed the thermal performance enhancement of a pristine eutectic salt of $LiNO_3$–KCl caused by the addition of functionalized GNPs for a solar absorption cooling storage system. The authors investigated the impact of the thermal conductivity enhancement on the design of the storage system, which is a PCM-based shell and tube heat exchanger. In Fig. 5, the thermal conductivity in the liquid phase is presented as a function of the filler content (red bars). The additivation of GNPs evidently influenced the effective thermal conductivity, reaching a maximum enhancement of 104% for 5% weight content of nanofiller. However, an effective reduction in the charging periods was not always obtained (blue bars in Fig. 5). Indeed, a significant reduction in the period required for the complete melting was observed only for the sample additivated with 5% weight content of nanofiller. This is attributed to the fact that the addition in a PCM matrix of nanofillers (and related surfactants required for the additivation processes) increases the viscosity of the liquid phase of the PCM, thereby resulting in a reduction in the convective heat transfer phenomena. Therefore, only the sample with 5% weight content of nanofiller adequately improved the thermal conductivity and compensated for the reduction in the natural convection to effectively reduce the charging period.

In a similar study, the efficiency enhancement resulting from the additivation of GNPs in a polyethylene glycol(PEG)-based matrix has been reported by He et al. [68]. The additivation of 2% weight content of GNPs evidently improved the charging and discharging periods of the storage system; nevertheless, the disadvantages represented by the increase in the viscosity (and reduction in the natural convection) were surpassed by the enhancement in thermal conductivity (that attained an improvement of up to 146%).

In addition to GNPs, other carbon-based nanofillers such as CNTs and carbon nanofibers (CNFs) have been used to enhance the thermal conductivity of phase change composites. In the study of Cui et al. [58], CNTs and CNFs have been added to soy wax-based matrices (up to 10% in weight). In Table 2, the comparison between thermal conductivity enhancements and charging periods for the samples additivated with CNFs and CNTs are reported. Although the CNTs exhibit higher thermal conductivity values in comparison to CNFs, the samples additivated with CNTs show a lower enhancement for all the considered contents. This lower enhancement obtained with CNTs is attributed to the worse dispersion and diffused entanglement that is typical of such nanotubes with high aspect ratios. In addition, similar results were observed in reducing the charging periods, which is reported as superior for the case of CNF fillers. The trend of the reduction in the charging periods of the soy wax-CNTs nanocomposite could be attributed to the increase in the effective viscosity of the nanocomposite. Such increase reduces the natural convection and hinders the reduction of the charging periods, if not properly overcome by an enhancement in the thermal conductivity.

A more comprehensive comparison between GNPs, short and long MWCNTs, and CNFs additivated in a paraffin matrix has been performed by Fan et al. [60] (weight content between 1% and 5%), wherein they reported negligible changes (maximum 1.1 °C) for the phase change temperatures in the samples additivated, whereas remarkable reduction in phase change enthalpies have been detected (up to 9.9% reduction at 5% CNFs concentration), as depicted in Fig. 6. The trend of the enthalpy in samples additivated with GNPs for both melting and solidification processes exhibited a drastic reduction with the additivation of 1% in weight, whereas slight variations were reported upon further increasing the filler content. A comparison between the thermal conductivity enhancement resulting from the additivation of 5% of nanofillers measured at 10 °C (solid phase) is presented in Fig. 7. As compared to the long CNTs, a superior enhancement was reported with short CNTs, which could be attributed to an improved dispersion of

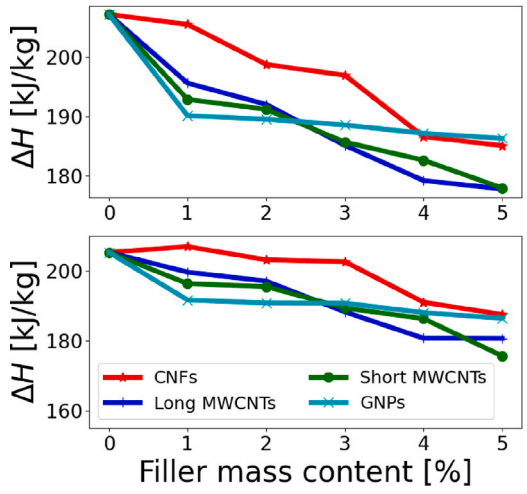

Fig. 6. Effect of weight content of various nanofillers on phase change enthalpies of a paraffin-based PCM during (top) charging and (bottom) discharging processes. ΔH is the phase change enthalpy [60].

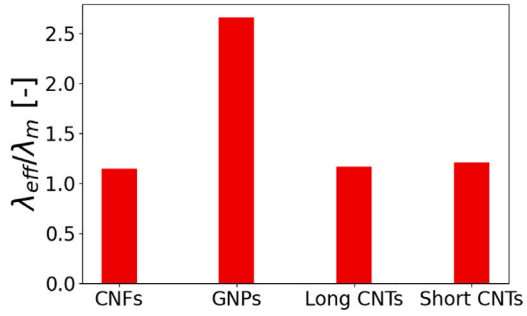

Fig. 7. Comparison between the effect of various nanofillers (5% weight content) on the effective thermal conductivity enhancement of paraffin-based nanocomposites. λ_{eff} is the effective thermal conductivity of the composite, λ_m is the thermal conductivity of the matrix alone [60].

the short CNTs inside the matrix. Moreover, among the nanofillers, the samples additivated with GNPs displayed outstanding enhancement in the thermal conductivity. This property may be attributed to the planar structure of GNPs, which limited the interface thermal resistances.

A vital parameter determining the effective thermal properties of nanocomposites is the percolation threshold, namely, the concentration at which the contact between the nanofillers inside the matrix occurs statistically [69]. The regime below the percolation threshold is called the *dilute* regime, whereas the one above is called the *percolating* regime [70]. In the dilute regime, the interfaces governing the thermal interface resistances are those between the filler and matrix. The impact of the interfaces between the fillers becomes predominant upon increasing the filler content. The nonlinearity of the effective thermal conductivity of nanocomposites as a function of the filler content is attributed to the switch between these two regimes. In the majority of the cases, in the percolating regime, the contact between the fillers creates a thermal path with low resistance, and consequently, a higher heat flux inside the nanocomposite, because the thermal interface resistances between the fillers are typically lower than those between the filler and matrix [70].

Notably, the surface functionalization used for reducing the thermal resistances at the interface between the fillers and matrix could be detrimental in the percolating regime. The coating generated by the functionalization could increase the thermal interface resistances between the fillers, which diminish the heat flux in the nanocomposite. An example of this phenomenon has been reported by He et al. [71], showing that the surface functionalization of the GNPs by polydopamine decreased the thermal interface resistance between the filler and the matrix. The sample additivated with functionalized GNPs exhibited higher thermal conductivity at a lower filler content (< 0.3% weight) as compared to that obtained with GNPs alone. For filler contents above 0.3% in weight, the sample additivated with GNPs presented a much higher thermal conductivity in comparison to the one additivated with coated GNPs. At 1% in weight content of GNPs, thermal conductivities of 0.78 and 0.93 W/m K were reported for the sample with coated GNPs and the one additivated with non coated GNPs, respectively.

Besides the enhancement in thermal conductivity, the addition of nanofillers generally leads to a reduction in the subcooling compared to bulk PCMs, as shown in Table 3. The additives, acting as nucleating agents, initiate the freezing process, thus leading to a higher onset freezing temperature with respect to that of the pure PCM [66]. The subcooling depends on several factors, such as the cooling rate, the presence of other impurities and the roughness of the container. For these reasons, a general trend in the subcooling reduction in Table 3 is absent. A recently published review about the impact of additives on the subcooling in PCMs for short-term applications can be found in the work by Shamseddine and coworkers [43].

2.2. Addition procedures

The addition procedure is essential for the effective thermal performance of PCM composites, as it influences the dispersion of fillers and the contact between fillers and matrix [72].

Several protocols have been reported for the production of PCM composites, as melt blending [73], mixing [74], and ball milling [73], but the most popular techniques are ultrasonication and magnetic stirring. The sonication process exploits acoustic waves to obtain the dispersion of fillers inside a matrix; for frequencies greater than 20 kHz, the process is referred to as ultrasonication. In the majority of existing research, ultrasonication is performed with the PCM in the liquid state, where the temperature is maintained above the melting one. As an example, Harikrishnan et al. [75] used a 40 kHz ultrasonication to disperse titanium dioxide nanoparticles in a stearic acid-based PCM, with a sonication period depending on the weight content of the filler in the PCM, e.g. it can vary between 20–45 min for content in weight of fillers ranging 0.05–0.3%. Additional liquids besides PCMs can be also employed for sonication: Singh et al. [59] performed a preliminary ultrasonication with functionalized GNPs additivated with gum acacia inside distilled water for 2 h. Subsequently, the PCM was added to the bath and further sonication was performed for 2 h. Finally, the temperature was raised up to 110 °C until the water evaporated. This process is graphically summarized in Fig. 8.

The magnetic stirring process, instead, exploits a rotating magnetic field to disperse the filler via a stir bar, immersed in the PCM in the liquid phase. This process has been exploited by Sunxi et al. [76] to mix expanded graphite with a PCM composed by an octanoic-myristic acid binary eutectic mixture. The PCM was initially heated up to a temperature greater than its melting temperature; subsequently, the stirring was performed for 30 min to achieve a uniform distribution of the PCM. Thereafter, the expanded graphite was inserted in the PCM and stirred every half an hour for six times to obtain a homogeneous dispersion.

Magnetic stirring and ultrasonication can also be used in sequence to obtain an improved dispersion of the nanofiller. As an example, this two-step method was exploited by Kumaresan et al. [66] to insert MWCNTs in a paraffin-based PCM. Initially, the fillers were homogeneously dispersed in the liquid paraffin using a magnetic stirrer (1 h) without using surfactants or dispersants. Successively, the mixture was sonicated in an ultrasonic bath for 30 min in isothermal environment above the melting temperature of the PCM. The resulting PCM, additivated with CNTs in weight content ranging from 0.15% to 0.6%, did not exhibit any visual sedimentation for at least 3 months. Ultrasonication and magnetic stirring were exploited in the melt-mixing

Table 3
Effect of additives on subcooling decrease in different PCM matrices for short term energy storage applications.

Nanoadditive	PCM	Nanoadditive content [%]	Subcooling decrease [%]	Ref.
MWCNT	Paraffin	0.15	37.44	Kumaresan et al. [66]
		0.3	19.17	
		0.45	18.26	
		0.6	19.63	
		1	8.82 (10.19)[a]	Fan et al. [60]
		2	2.41 (3.99)[a]	
		3	3.68 (1.16)[a]	
		4	12.95 (10.32)[a]	
		5	−0.21 (−0.11)[a]	
CNF	Paraffin	1	−5.10	Fan et al. [60]
		2	8.81	
		3	10.07	
		4	14.16	
		5	5	
GNP	Eutectic PCM	1	10	Singh et al. [67]
		3	22	
		5	32	
	PEG	0.5	11.78	He et al. [68]
		1	10.27	
		1.5	6.04	
		2	14.20	
	Paraffin	1	8.87	Fan et al. [60]
		2	14.10	
		3	10.40	
		4	6.65	
		5	10.05	

[a]Refers to short MWCNT.

Table 4
Summary of the major additivation techniques present in the literature.

Process	Filler	PCM	Filler content	Ref.
Magnetic stirring	Expanded graphite	Octanoic-myristic acid binary eutectic mixture	7% wt.	[76]
Ultrasonication	Titanium dioxide	Stearic acid	0.05–0.3% wt.	[75]
Ultrasonication + magnetic stirring	MWCNTs	Paraffin	0.15–0.6% vol.	[66]
	Carbon black nanopowder–Nickel nanoparticles–Copper nanoparticles–Silver nanowires–MWCNTs–GNPs	Hexadecane	0.001–0.01% wt.	[77]
	CNTs–CNFs	Soy–paraffin	1%–10% wt.	[58]
	MWCNTs - GNPs - CNFs	Paraffin	1%–5% wt.	[60]

protocol by Fan et al. [60], who adopted a dispersion step followed by a solidification step, as schematically represented in Fig. 9. In the former step, the molten paraffin additivated with CNFs was stirred for 15 min and ultrasonicated for 50 min. During the dispersion, the temperature was maintained above the melting point of the paraffin. In the latter step, the mixture was solidified in a mold at room temperature. A melt–mixing procedure was performed by Cui et al. [58], who added CNFs and CNTs in soy or paraffin-based PCMs. After stirring for 30 min, the mixture was ultrasonicated for 1 h. Ultimately, the mixture was poured into a mold at room temperature. Mishra et al. [77] added different nanoinclusions in a hexadecane PCM. First, the surfaces of the nanofiller were functionalized with oleic acid via sonication (20 min) and magnetic stirring (40 min); subsequently, the mixture was washed and centrifuged to remove the excess oleic acid. Ultimately, the functionalized nanofillers and PCM were sonicated in a horn sonicator for 5 min.

The various processes, fillers, and matrices used for obtaining composite PCMs are summarized in Table 4: the two-step method leads to a better dispersion of the nanofillers inside the PCM matrix. For such reason, it is the most diffused additivation technique [38].

3. Subcooling

A promising application for PCMs is related to long-term TES that exploits the deep subcooling effect of certain materials for storing the latent heat for long periods without heat losses [78]. Subcooling is a metastable state that occurs when a material—during the cooling or heating process—intercepts a metastable phase transition temperature and does not solidify or melt [79]. In particular, subcooling can be categorized as a kinetic property [80], and the degree of subcooling (T_{sc}) is defined as the difference between the melting temperature (T_m) and solidification temperature (T_s), i.e., $T_{sc} = T_m - T_s$ [81]. Subcooling phenomena can be categorized into heterogeneous and homogeneous subcooling. In heterogeneous subcooling, the solidification starts in preferential sites such as impurities or imperfections on the boundaries [82], whereas in homogeneous subcooling, crystals are formed within the bulk liquid. In the latter, the free-energy barrier to be surpassed for enabling the spontaneous growth of the new phase is much higher than the one required for heterogeneous solidification [78,82]. For instance, even if the melting point of water at atmospheric pressure is around 273 K, extremely pure water can be subcooled to 232 K [83]. The degree of subcooling and its stability depends on several factors, such as: presence of impurities in sample; dimensions of sample volume; container geometry and surfaces roughness; cooling rate; heating temperature above melting point at which the sample is exposed [81,84].

In general, a majority of the PCMs for thermal storage applications exhibit subcooling. This phenomenon is less evident in organic PCMs such as paraffins and fatty acids than in inorganic PCMs such as salt

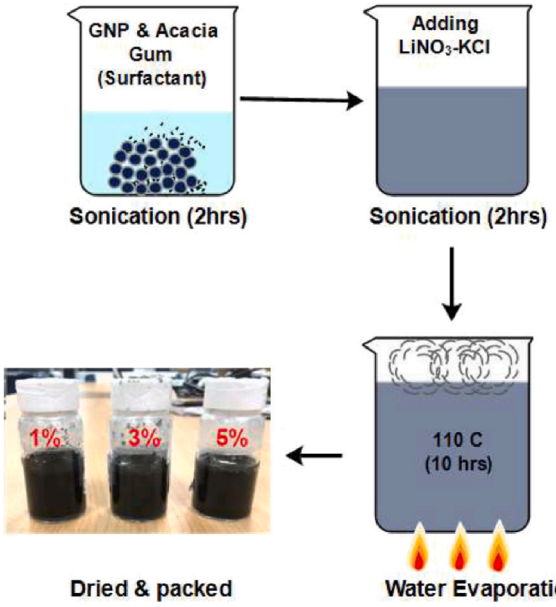

Fig. 8. Summary of additivation technique performed in Ref. [59]. After a preliminary ultrasonication of GNPs and immersion of surfactants in water, the paraffin-based PCM was added to the mixture for further ultrasonication. Eventually, the sample was heated until the water evaporated, obtaining the nanocomposite samples shown in the image at the bottom left.
Source: Image sourced from Ref. [59].

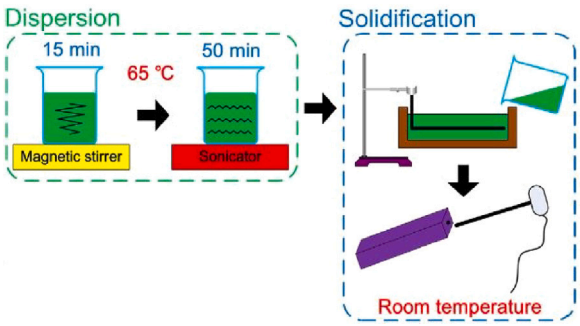

Fig. 9. Summary of the two-step method used in Ref. [60] to additivate CNFs to a paraffin-based PCM. The dispersion method including magnetic stirring and sonication is followed by solidification of the composite in the mold.
Source: Image modified from Ref. [60].

hydrates. The subcooled state is usually not desirable for short-term thermal energy storage solutions, and several studies have attempted to minimize or avoid it, specifically because the latent heat of fusion is not released during subcooling and the material requires additional energy for the phase transition, thereby reducing the storage process efficiency [81,85]. This particular characteristic can be exploited, instead, for long-term thermal storage: once the material is in the liquid state, it can be cooled below its melting temperature. In this metastable state, the latent heat remains stored until an external source triggers the exothermic solidification process [78]. It is worth to note that various additives can be added to PCMs to either increase or decrease the subcooling [86,87].

Although subcooling is a typical property of liquid–solid PCMs, it has been recently studied also in solid-to-solid PCMs (SSPCMs) for long-term heat storage [88,89].

In this section, we review the above-mentioned phase-change materials that exhibit a deep subcooling and can be used for low-temperature thermal energy storage applications, such as sodium acetate trihydrate (SAT) and sugar alcohols (SA) along with their

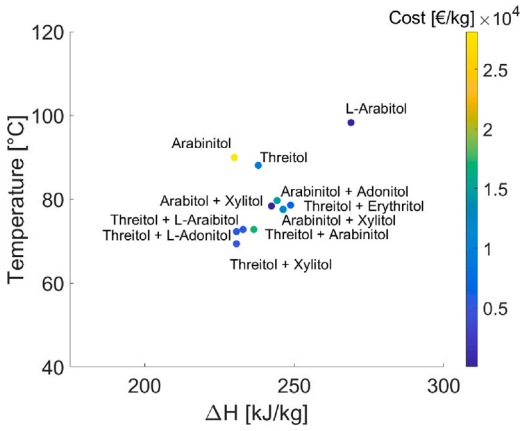

Fig. 10. Overview of SAT and SA materials with cost in thousands of Euros per kg. ΔH refers to latent heat of fusion. References for costs: threitol [90], arabinitol [90], l-arabitol [90], adonitol [90].

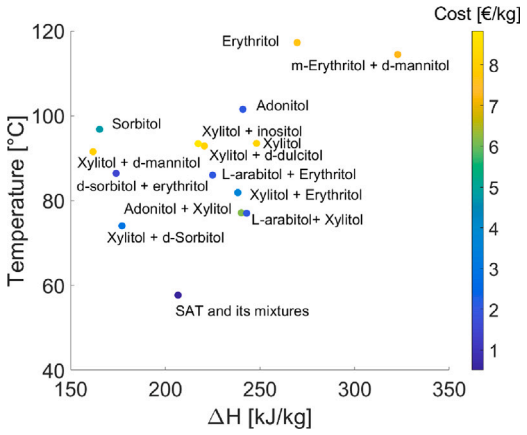

Fig. 11. Overview of SAT and SA materials with cost in a few Euros per kg. ΔH refers to latent heat of fusion. References for costs: SAT [91,92], xylitol [90,93–95], erythritol [90,93,94], sorbitol [93], d-dulcitol [90], inositol [90], d-sorbitol [23,90], d-mannitol [90].

mixtures. An overview of the cost, transition temperature, and latent heat of fusion of various SATs and SAs is presented in Figs. 10 and 11. The reported costs refer mainly to materials with high purity (at least >97%). In the case of large quantities of those products to be used for thermal energy storage purposes, an extremely high purity may not be necessary. If so, it might be possible to find cheaper products for instance from wholesale stores.

3.1. Sodium Acetate Trihydrate (SAT)

The Sodium Acetate Trihydrate (SAT) is an inorganic salt hydrate with chemical formula $NaC_2H_3OO \cdot 3\,H_2O$, and its standard composition by weight is 60.3% of sodium acetate and 39.7% of water. SAT is a promising candidate material for low-temperature TES owing to its low cost, high latent heat of fusion (264–289 kJ/kg), and melting temperature (58–58.4 °C). Moreover, it is nontoxic and noncorrosive [96,97]. As a salt hydrate, its thermal conductivity of 0.6 W/m K is relatively high in comparison to the organic PCMs, which yields shorter charge and discharge times [35,98]. Ultimately, SAT exhibits a significant degree of subcooling and can be easily subcooled below 0 °C. However, the dehydration of SAT gradually initiates from 125 °C up to 160 °C, where all the water contained in the hydrated salt is lost and the material loses its storage capabilities [99]. SAT has been extensively studied for short-term applications with additives and

Table 5
Thermal properties of SAT in literature. Data without temperatures in parentheses are stated without reference temperature.

Reference	Melting point [°C]	Heat content [kJ/kg]	Density solid [kg/m^3]	Density liquid [kg/m^3]	Specific heat solid [kJ/kg K]	Specific heat liquid [kJ/kg K]	Thermal conductivity solid [W/m K]	Thermal conductivity liquid [W/m K]
Ouchi et al. [118]	–	–	–	1287 (T = 61 °C)	–	3.00 (T = 61 °C)	–	0.416 (T = 61 °C)
Abhat [119]	58	250	–	–	–	–	–	–
Meisingset and Grønvold [97]	58	278	–	–	1.77 (T = 40 °C)	–	–	–
Araki et al. [98]	58	257 (T = 40 °C)	–	–	2.05 (T = 30 °C)	3.00 (T = 70 °C)	0.69 (T = 30 °C)	0.36 (T = 70 °C)
Sandnes and Rekstad [120]	–	226	–	–	–	2.79	–	–
Wada et al. [121]	58.4	264	–	–	1.70	2.90	–	–
Wei and Ohsasa [110]	58	205	–	–	–	–	–	–
Kaizawa et al. [99]	59	156–331	–	–	–	–	–	–
Zhou and Xiang [30]	58	265	1450	1280	–	–	–	–
Zhou et al. [31]	53	–	–	–	–	–	–	–
Dannemand et al. [113]	–	–	–	–	–	–	0.68	–
Dannemand et al. [113]	–	–	–	–	–	–	0.59	–
Li et al. [122]	–	–	–	1282 (T = 70 °C)	–	2.99 (T = 70 °C)	–	0.44 (T = 70 °C)
Beaupere et al. [123]	–	253	–	–	2.021	3.260	–	–

various strategies to reduce the subcooling effect [100–109], and for long-term storage purposes to exploit its high degree of subcooling [96,110,111]. In particular, Furbo et al. has delivered considerable efforts in characterizing the material and scaling up this storage technology by combining SAT-based storage with solar collectors and domestic hot-water systems [91,92,112–117].

The SAT properties from various references are listed in Table 5. Note that certain authors report the "latent heat of fusion", whereas others use "enthalpy change" or similar terms; thus, we merged these quantities under the label of "heat content" for an easier data interpretation. The scattering of the referenced data is due to the different experimental methods adopted. For example, Sandnes and Rekstad [120] measured the latent heat by using cylindrical glass tubes 10.7 cm high with a 1.58 cm diameter placed on insulating polystyrene. On the other hand, Wada and coworkers [121] measured the SAT in a stainless steel vessel, with 3 cm inner diameter and 10 cm high. The vessel was sealed and put into a water bath. A more detailed description of the prototypes available in literature is provided in the next sections.

Note that certain authors [124] report the heat content of the subcooled sample, which was lower than the latent heat owing to the heat capacities varying between the liquid and solid state of SAT. The broad use of SAT is still limited by certain significant challenges such as cycling stability and low thermal conductivity. Thus, various approaches such as the addition of water or other additives to the SAT solution have been investigated and are discussed below.

3.1.1. Addition of water

The addition of water to the SAT improves the dissolution of the salt, thereby reducing precipitation and yielding a moderate enhanced cycling stability. Water addition may also increase the subcooling degree [123], whereas a higher water content reduces the heat storage potential of the solution, given that a part of the PCM is substituted by water [84]. However, optimizing the heat content as a function of water is not a trivial task, since different experimental methods give different results, as reported in Table 6. For example, Beaupere and coworkers [123] used 250 cm^3 polymethyl methacrylate (PMMA) bricks that contain 350 g of SAT and thermal cycles of 8 h were applied. On the other hand, Kong and coworkers [125] employed plastic bottles of different heights. They investigated phase separation and heat content of the subcooled SAT at various concentrations (40%, 42%, 45%, and 46% weight content of water). After heating the mixtures between 80 °C and 85 °C, they exposed the samples to indoor ambient temperature and maintained them in a subcooled state for more than four months. After the solidifying phase, each sample was cut in 3 or 4 horizontal layers that were subsequently analyzed. The mixture with 40% water content was affected by phase segregation for all the sample bottles tested (4, 5, and 8 cm heights). However, the samples with 42% content of additional water were affected by the phase separation only in the 8 cm bottles. Zhou and coworkers [30] report stable subcooling for salt–water ratios of 3:2, 1:1, and 2:3 SAT–water mixtures (including the original crystal water in the sodium acetate trihydrate). In a separate experimental work, Kong et al. [124] used the heat loss method to compare the heat contents of SAT with water or thickeners. The tested samples were 5 cm in height, and only the samples with a water content higher than 42% did not exhibit visible segregation. The properties of the SAT–water solutions are listed in Table 6 as a function of water content.

3.1.2. Addition of thickeners

The addition of thickeners to a SAT solution can alleviate the segregation problems. In particular, a low weight content (1%–2%) is sufficient for improving the stability of SAT with a low impact on the latent heat of the composite material. In SAT-based mixtures, the most commonly used thickeners are carboxymethyl cellulose (CMC) and the Xantham gum (X-Gum). Water is not commonly added with thickeners, as the additional water would dilute the thickener and hinder its influence. Kong et al. [124] report that SAT solutions with CMC or X-Gum in weight contents up to 2.0% remarkably increase the heat content up to 215 kJ/kg with respect to samples with additional water. A more detailed comparison is reported in Fig. 12.

Ryu et al. [32] reported that the addition of CMC to SAT mixtures in weight contents between 2.0% and 3.0% assures thermal stability over 300 cycles. However, this thermal cycling measurements were recorded in the presence of nucleating agents, as the research focused on short-term latent thermal energy storage. Furthermore, the authors reported that the subcooling degree of the unthickened SAT without a nucleating agent was beyond 30 °C. The addition at low weight percentage of thickeners is therefore desirable to improve the stability by reducing the segregation issues.

3.1.3. Addition of fillers

The relatively low thermal conductivity of the SAT may be improved by adding highly conductive materials such as graphite nanoparticles. However, these particles may precipitate from the solution owing to their higher density. Moreover, these additives may act as nucleation centers for the spontaneous triggering of the subcooled solution. Therefore, thickeners are typically added together with the graphite to obtain

Table 6
Dependence of SAT–water solution properties on water content (water content % by weight). Data without temperatures in parentheses are stated without a reference temperature.

Weight content of water [%]	Melting point [°C]	Heat content [kJ/kg]	Specific heat solid [kJ/kg K]	Specific heat liquid [kJ/kg K]	Thermal conductivity solid [W/m K]	Thermal conductivity liquid [W/m K]	Reference
40.0	–	162	–	–	–	–	Kong et al. [125]
42.0	58	–	–	–	–	–	Fan et al. [126]
42.0	–	194	–	–	–	–	Kong et al. [125]
42.0	–	214	–	3.20	–	–	Beaupere et al. [123]
42.7	58	360	–	–	–	–	Froese [127]
43.0	–	177	–	–	–	–	Dannemand et al. [112]
44.0	58	185	2.17 (T = 30 °C)	3.14 (T = 70 °C)	0.58 (T = 30 °C)	0.37 (T = 70 °C)	Araki et al. [98]
45.0	–	165	–	–	–	–	Kong et al. [125]
45.1	–	–	–	–	–	0.64	Dannemand et al. [113]
45.1	–	–	–	–	–	0.56	Dannemand et al. [113]
46.0	–	159	–	–	–	–	Kong et al. [125]
46.7	55	243	3.13	3.28	–	–	Sandnes and Rekstad [120]
49.7	63	169.7	–	–	0.37	–	Yuan et al. [84]
54.7	58	72	–	–	0.68	0.40	Araki et al. [98]

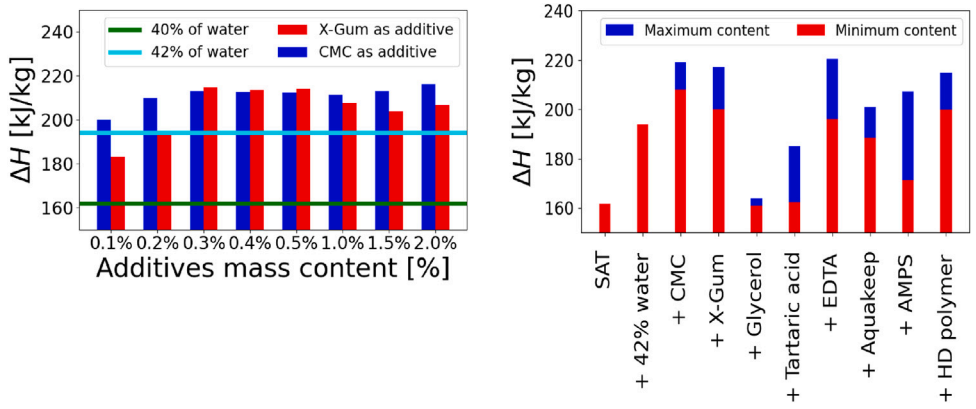

Fig. 12. Enthalpy content of SAT with various additives. Minimum and maximum content refer to the content of each tested additive. ΔH is the phase change enthalpy [124,125].

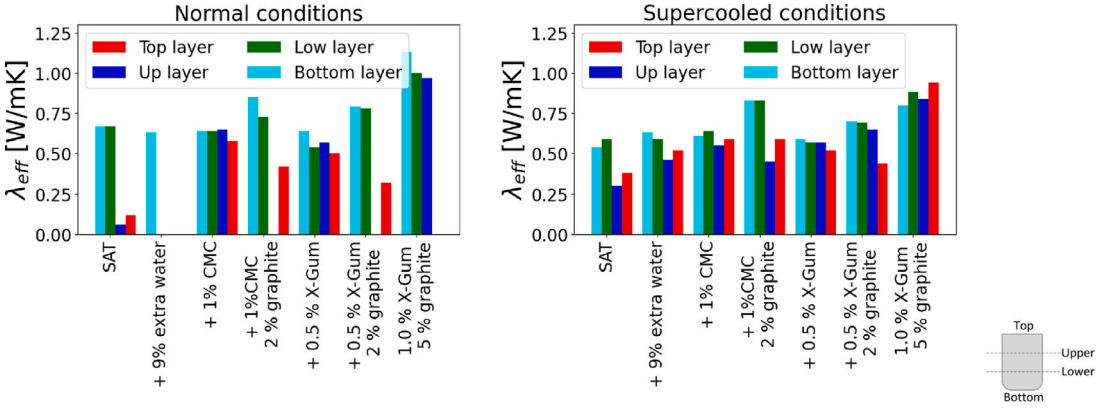

Fig. 13. Thermal conductivity of SAT mixtures for normal (left) and supercooled (right) conditions. Values measured for 4 sample slices (gray schematic) with thickness of each layer at 25–30 mm. PCM samples were 90–100 mm high with a diameter of 120 mm. λ_{eff} is the effective thermal conductivity of the composite [113].

a more stable solution. Dannemand et al. [113] prepared multiple SAT samples with varying solution compositions and compared the thermal conductivity measured at various positions in the sample. The results, summarized here in Fig. 13, demonstrated an increase of up to 39% in thermal conductivity with samples of 1% graphite content.

3.1.4. Prototypes

Studies on prototypes using SAT for TES were conducted by Furbo et al. who analyzed different tank shapes and their performance, as shown in Fig. 14. In particular, prototypes comprising a flat rectangular unit (1.2 m × 2.4 m × 0.05 m) were constructed [91,92]. One of the prototypes was filled with 200 kg SAT with 9% additional water, and the heat discharged after solidification of the subcooled PCM at ambient temperature was 194 kJ/kg in the first test cycle and 179 kJ/kg after 20 test cycles. However, the crystallization started spontaneously during the discharge in 13 of the 20 test cycles. This phenomenon could be attributed to the inadequately low temperatures in the SAT caused by extremely short charging periods or by the clogging of the PCM in the device. On the contrary, the energy discharged for the SAT and CMC mixture was stable at approximately 205 kJ/kg of PCM over six

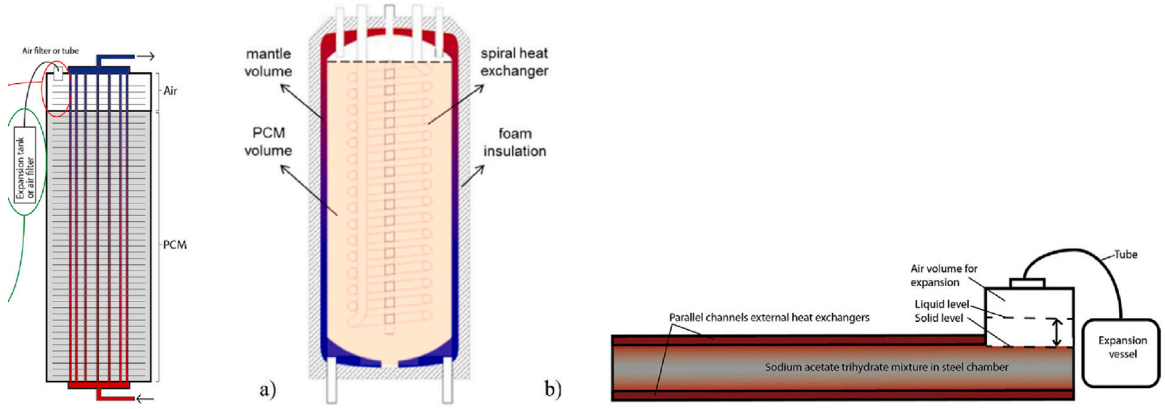

Fig. 14. Various storage configurations of tanks containing SAT. Left to right: cylinder [112], cylinder tank-in-tank [115], flat [128].
Source: Images modified from Refs. [112,115,128].

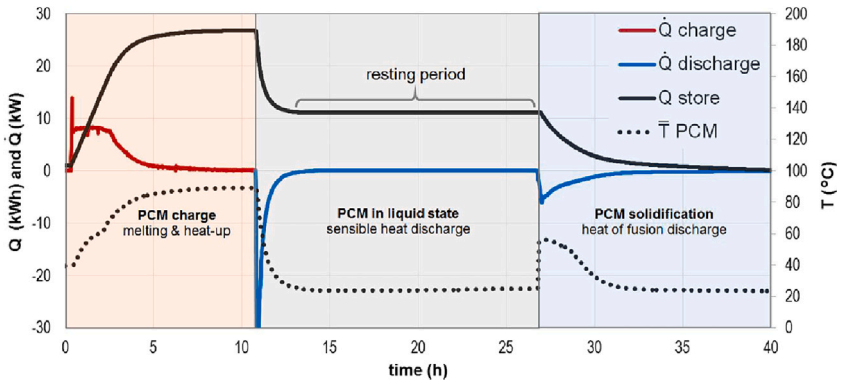

Fig. 15. Time evolution of heat content, thermal power and temperature during the 5th heat storage test cycle with SAT composite conducted in Ref. [115].
Source: Image sourced from [115].

test cycles. In this case, the crystallization started spontaneously in two of the six test cycles.

In Ref. [112], two 116-kg-solutions of SAT—one with 4.4% weight content of graphite along with 0.5% X-Gum (SATXC), and the other containing SAT with 6.4% additional water (SATH2O)—were tested in a 1.5-m-high cylindrical heat storage. The heat discharged after the solidification of the subcooled SATXC was 24–26 MJ (about 206–224 kJ/kg) for the test cycles, wherein the stable subcooling was achieved. The subcooled state for the SATH2O was attained in 7 of the 17 test cycles. In contrast, the SATXC achieved a subcooled state at ambient temperature in only 6 of the 40 test cycles. The segregation issues already experienced with small samples became relevant in this configuration, i.e., the heat discharged after the solidification decreased from 177 kJ/kg (measured in the first cycle) to 140 kJ/kg (measured in the 17th test cycle).

Another 1.2-m-high cylindrical prototype with a tank-in-tank configuration containing 200 kg of SAT composite with 2% water by weight and 3% liquid polymeric solution by weight was developed and tested by the same group (refer to Figs. 14 and 15). The authors performed 12 test cycles in which they obtained low subcooling temperatures. Moreover, the energy discharged in the subcooled PCM was approximately 41.4 MJ, corresponding to 207 kJ/kg.

3.1.5. Production processes

Dannemand et al. [112,113] prepared a remarkable quantity of SAT and water by melting the solid SAT in a closed barrel inside an oven at 90 °C for one or several days and, subsequently, adding water to the solid SAT. Notably, the additivation of 1% in weight of demineralized water to the granulated SAT has been reported to completely dissolve the SAT [27].

Although the addition of excess water is a straightforward process, various procedures are also reported for the additivation of thickeners. Thus, appropriate mixing methods are required to obtain a homogeneous dispersion of the thickening agents, i.e., CMC and X-Gum, inside the SAT mixture. The facile binding between thickeners and water, especially with the X-Gum, produces jelly chunks [124], which reduce the properties of the PCM. To avoid this limitation, thickening agents were mixed in the form of powder with a fraction of the total SAT in a cold solid granular state. Subsequently, this mixture was added in small portions to the remaining fraction of SAT, which was in the liquid phase [113]. During this process, a continuous stirring was performed. The mixing was carefully performed to avoid the formation of air bubbles in the mixture, which would reduce both the storage density and heat transfer [112,113]. In addition, this mixing process could be performed using a mortar mixer (with a moderate intensity, because the mixture is in the form of a thick jelly) [112] by means of shaking the container of the additivated solid SAT [129] or with the use of an overhead mixer [113].

Another reported procedure entails the progressive additivation of the thickener (e.g., CMC) in the liquid SAT by mechanical stirring [112]. In this case, a minimum content of 1% CMC is required to obtain a stable, uniform mixture [112]. Subsequently, the mixture with the thickeners can be heated to obtain a uniform temperature [112,113]. Similar processes are adopted for several additives, i.e., small portions of polymers can be gradually added into the melted SAT while stirring with an electronic stirrer [124] or by inserting the liquid polymer using pipettes and performing the stirring afterward [27]. Graphite is usually mixed before placing the SAT in the oven and starting the entire process, as discussed in Section 2.

3.2. Sugar Alcohols (SAs)

Sugar Alcohols (SAs), also referred to as polyalcohols or polyols, constitute a subclass of carbohydrates and are characterized by an alcohol group at the location of the carbonyl group in the aldose and ketose moieties of mono-, di-, oligo- and polysaccharides. Generally, SAs are formed by polar molecules that generate a network of hydrogen bonds in the crystal, yielding remarkable intermolecular forces [130]. In addition, most of the SAs are produced by chemical reduction of carbohydrates; their market price can be as low as 1–6 €/kg [23], and a majority of the sugar alcohols are noncorrosive and nontoxic [131]. Although these materials are typically used as sweeteners in the pharmaceutical and food industries, they have been recently proposed as PCM candidates owing to their high latent heat between 240 and 340 kJ/kg and melting temperatures within 90–200 °C (refer to Table 7). Moreover, the eutectic mixtures of two or more SA may be prepared to use these materials for low-temperature thermal energy storage applications, as an eutectic mixture exhibits a lower melting point in comparison to its constituent [130]. A majority of the SAs present a severe and stable subcooling, so they may be suitable for long-term thermal energy storage applications. The SAs typically present polymorphism, indicating that they can form amorphous metastable phases reflecting various thermophysical and chemical properties [93]. The presence of these various phases during the solidification process depends on several factors, such as the presence of additives, solvent type, temperature range, temperature gradient, and preparation method [130]. The melting temperature of SAs is beyond 75 °C [90] owing to the high strength of their crystal lattice as compared to alternative materials.

The extensively studied SAs for thermal energy storage applications include erythritol, xylitol, and D-mannitol, regardless of more than 900 SAs listed in the dictionary by Collins [132].

Recently, erythritol has been studied as a PCM for short-term applications in waste-heat transportation [133], absorption chillers [134] and in the automotive sector [135]. The erythritol ($C_4H_{10}O_4$) is characterized by a melting temperature of approximately 118 °C and latent heat of 340 J/g [136]. However, certain authors [94] reported a lower melting temperature of 105.1 °C, probably because of the occurrence of various crystal structures within the solid phase during the experiments. The same authors reported a thermal conductivity of 0.89 ± 0.06 W/m K and 0.33 ± 0.02 W/m K for the solid (20 °C) and liquid (140 °C) phases, respectively. The erythritol demonstrates appropriate thermal stability for cycles up to 1000 [137] and starts decomposing above approximately 160 °C. The degree of subcooling reported for erythritol varies between 14 °C [137] for a sample size of 200 g and 82 °C [138] for a sample size of a few milligrams. This variation is caused by the potential presence of greater amount of impurities acting as nucleation sites in larger samples (see Fig. 16).

In comparison, xylitol ($C_5H_{12}O_5$, (2S,4R)-pentane-1,2,3,4,5-pentol) is more dense (1500 kg/m^3), noncorrosive, and exhibits subcooling. Its melting temperature is approximately 90 °C and its latent heat is greater than 230 kJ/kg. The thermal conductivity values for xylitol are 0.5 W/m K for the solid phase and 0.3 – 0.4 W/m K for the liquid phase. However, the major limitation of xylitol is its relatively slow crystallization that causes a low release rate of the latent heat [139]. Among sugar alcohols, xylitol is a promising material for long-term low-medium temperature heat storage, since it is relatively cheap (as shown in Fig. 11) and its melting point is below 100 °C. As compared to alternative SAs, D-mannitol is nontoxic and relatively cheap (2 €/kg) [140,141]. In addition, D-mannitol exhibits a high melting temperature of 167 °C and a heat of fusion of 328.8 kJ/kg. However, the presence of a metastable phase may modify its thermal properties. Barreneche et al. [142] performed some differential scanning calorimetry analysis and have reported that only one melting point (167 °C) exists during the first heating test cycle, which corresponds to the presence of the β phase. A lower heat of fusion, characteristic of the metastable δ phase,

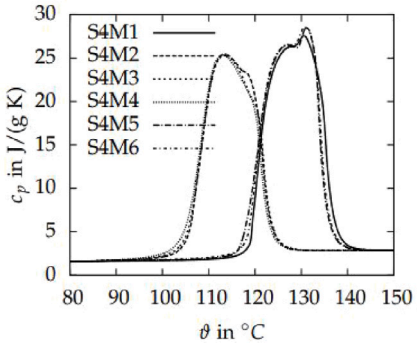

Fig. 16. Heat capacity of erythritol as a function of temperature for various melting cycles (M1–M6) for the same sample. Two distinct melting points depend on crystal structure of solid phase during each cycle [94].
Source: Image sourced from Ref. [94].

was reported for the following cycles. Mojiri et al. [143] reported a degradation temperature of 207 °C, in contrast to the 300 °C measured by Kumaresan et al. [141]. As this temperature is proximate to the melting point (167 °C), it could represent a limiting factor in the application of D-mannitol. During the melting process, local overheating due to the low thermal conductivity may cause partial degradation of the material. Solé et al. [140] reported a 50% reduction in enthalpy at the 50th cycle with oxygen in the environment, whereas no variations were observed in its properties in absence of oxygen. On the other hand, Rodríguez-García et al. [144] reported that slight degradation is present in environments without oxygen. Moreover, the heat of fusion decreased during the heating/cooling cycles, i.e., a 15% degradation of the fusion heat (from 293 kJ/kg to 245 kJ/kg) was measured at the 100th cycle. Neumann et al. [145] have proposed a theory for the degradation of D-mannitol, according to which the presence of oxygen in the environment determines the rate of degradation of the melting enthalpy. Nevertheless, to some extent, degradation occurs also in the absence of oxygen owing to the production and separation of certain degradation products such as cyclic ether 2,5-anhydro-D-mannitol.

3.2.1. Eutectic mixtures

The melting temperature of SAs (see Table 7) is generally above 90 °C, which limits their use with low-temperature heat sources such as solar collectors or waste heat. Thus, eutectic mixtures of various SAs have been studied to surpass this limitation. Several eutectic mixtures with a melting temperature well below 80–85 °C and a latent heat spanning from 170–250 kJ/kg have been studied (see Table 8). Additionally, the phase diagrams of certain eutectic mixtures are presented in Fig. 17. Notice that the specific heat and thermal conductivity do not vary significantly between the single SAs and their eutectic mixtures. Furthermore, the degradation rates of eutectic mixtures are significantly smaller than those of single component sugar alcohols [130].

However, the crystallization rate of these mixtures is lower than that of the individual components, which may limit applications requiring higher charge and discharge powers.

As Fig. 18 shows, the maximum crystallization rate of the erythritol–xylitol eutectic mixture is one order of magnitude lower than that of the pure xylitol, whose crystallization rate is not exceptionally high. The theory from Winegard et al. [146] can explain the low crystallization rate of the eutectic mixtures, according to which the crystallization starts with the nucleation of one of the phases. In particular, this phase grows until the surrounding liquid is enriched in other components and, at this instant, an alternate nucleation of the two phases occurs until the solidification process is concluded.

Table 7
Thermophysical properties of sugar alcohols used as phase change materials. Data without temperatures in parentheses are stated without reference temperature.

	$T_{melting}$ [°C]	Heat content [kJ/kg]	Density liquid [kg/m^3]	Density solid [kg/m^3]	Specific heat solid [kJ/kg K]	Specific heat liquid [kJ/kg K]	Thermal conductivity solid [W/m K]	Thermal conductivity liquid [W/m K]	Supplier	Reference
d-dulcitol (or galacticol)	185.9	334.1	–	–	–	–	–	–	Macklin	[90]
d-dulcitol (or galacticol)	187.3	350.8	–	–	–	–	–	–	Aladdin	[90]
Inositol	224.3	258.3	–	–	–	–	–	–	Sigma Aldrich	[90]
Inositol	224.5	261.8	–	–	–	–	–	–	Aladdin	[90]
D-mannitol	166	286.1	1490	–	1.38	–	–	–	–	[145]
D-mannitol	166	281	–	–	–	–	–	–	–	[90]
D-mannitol	166	297	–	–	1.30	–	0.6	–	–	[143]
D-Threitol	87	251	–	–	–	–	–	–	–	[147]
D-Threitol	88.7	225	1386 (T = 20 °C)	1299 (T = 100 °C)	1.28 (T = 20 °C)	2.4 (T = 100 °C)	0.73 (T = 20 °C)	0.48 (T = 100 °C)	–	[148]
L-Threitol	88.6	238	–	–	–	–	–	–	–	[90,130]
Adonitol	102	220	–	–	–	–	–	–	–	[90,149]
Xylitol	90	237.6	1505 (T = 20 °C)	1344.6 (T = 120 °C)	1.27 (T = 20 °C)	2.73 (T = 120 °C)	0.52 (T = 20 °C)	0.36 (T = 140 °C)	Hamburg Fructose GmbH International	[94]
Xylitol	93.4	237.5	–	–	–	–	–	–	Sigma Aldrich	[90]
Xylitol	93.3	231.4	–	–	–	–	–	–	Aladdin	[90]
Xylitol	94.7	240.1	–	–	–	–	–	–	Alfa Aesar, purity 99%	[93]
Xylitol	93	263	1497 (T = 20 °C)	1328 (T = 100 °C)	1.24 (T = 20 °C)	2.6 (T = 100 °C)	1.3 (T = 25 °C)	0.4 (T = 90 °C)	Roquette, purity 98.43%)	[150,151]
Xylitol	95.1	267	1500 (T = 20 °C)	1329 (T = 100 °C)	1.252 (T = 25 °C)	2.602 (T = 100 °C)	1.31 (T = 27 °C)	–	Roquette, Purity 99.43%	[95]
Xylitol	95.1	251	–	–	–	–	–	–	Sigma-Aldrich, Purity 99%	[130]
Xylitol	94.5	258	–	–	–	–	–	–	–	[152]
Xylitol	94	252	–	–	–	–	–	–	–	[153]
Xylitol	93	280	–	–	–	–	–	–	–	[99]
Xylitol	–	164	–	–	–	–	0.37 (T = 20 °C)	0.41 (T = 110 °C)	–	[154]
Xylitol	92	259	–	–	–	–	–	–	–	[139]
Erythritol	110	–	–	–	–	–	–	–	–	[90,110]
Erythritol	117.1	310	–	–	1.214 (T = 20 °C)	2.639 (T = 132 °C)	–	–	–	[136]
Erythritol	117	344	–	–	–	–	–	–	–	[99]
Erythritol	–	229	–	–	–	–	0.59 (T = 20 °C)	0.32 (T = 125 °C)	–	[154]
Erythritol	118	315	–	–	1.02	–	–	–	–	[155]

(*continued on next page*)

Table 7 (*continued*).

Erythritol	118.1	352.9	1440.4 (T = 20 °C)	1289.1 (T = 120 °C)	1.34 (T = 20 °C)	2.87 (T = 150 °C)	0.89 (T = 20 °C)	0.33 (T = 140 °C)	Hamburg Fructose GmbH International	[94]
Erythritol	118.7	333.7	–	–	–	–	–	–	Alfa Aesar, purity 99%	[93]
Erythritol	118.2	340	1480 (T = 40 °C)	1345 (T = 130 °C)	1.18 (T = 20 °C)	1.69 (T = 140 °C)	0.76 (T = 20 °C)	–	Cargill, Purity 99.5%	[95,156]
Erythritol	119	340	1480 (T = 20 °C)	1300 (T = 140 °C)	1.38 (T = 20 °C)	1.77 (T = 140 °C)	0.73 (T = 20 °C)	0.33 (T = 140 °C)	Mitsubishi Chemical Corp., Purity > 99.5%	[157]
Erythritol	117	339	–	–	–	–	–	–	–	[137]
Erythritol	118.9	332.3	–	–	–	–	–	–	Energy Chemical	[90]
D-Arabitol	–	144.6	1470 (T = 25 °C)	–	–	–	–	–	–	[90,150]
D-Arabitol	104	246.8	–	–	–	–	–	–	–	[130]
L-Arabitol	101.9	247	–	–	–	–	–	–	–	[90,95]
L-Arabitol	90	280	–	–	–	–	0.93	0.41	–	[158]
L-Arabitol	103	280	1563 (T = 30 °C)	1300 (T = 100 °C)	0.967 (T = 25 °C)	1.554 (T = 100 °C)	0.93 (T = 27 °C)	0.41 (T = 120 °C)	Standford Chem., Purity 98%	[95]
L-Arabinitol	90	230	–	–	–	–	–	–	–	[90]
Adonitol	103	250	–	–	1.586 (T = 20 °C)	1.541 (T = 120 °C)	0.37 (T = 60 °C)	0.42 (T = 100 °C)	Sigma Aldrich, Purity > 99%	[95]
Adonitol	100	232	–	–	–	–	–	–	Sigma Aldrich, Purity > 99%	[130]
Sorbitol	97.6	153	–	–	–	–	–	–	Sigma Aldrich, Purity > 99.5%	[93]
Sorbitol	93.3	174	–	–	–	–	–	–	Brenntag	[153]
Sorbitol	97	110	–	–	–	–	–	–	–	[99]
D-sorbitol	97.4	164	–	–	–	–	–	–	Sigma Aldrich	[90]
D-sorbitol	99.4	184.4	–	–	–	–	–	–	Aladdin	[159]
D-sorbitol	95	187	1525	–	–	2.50	–	–	–	[160]
D-sorbitol	97.7	185	1500 (T = 20 °C)	–	–	–	–	–	–	[23]

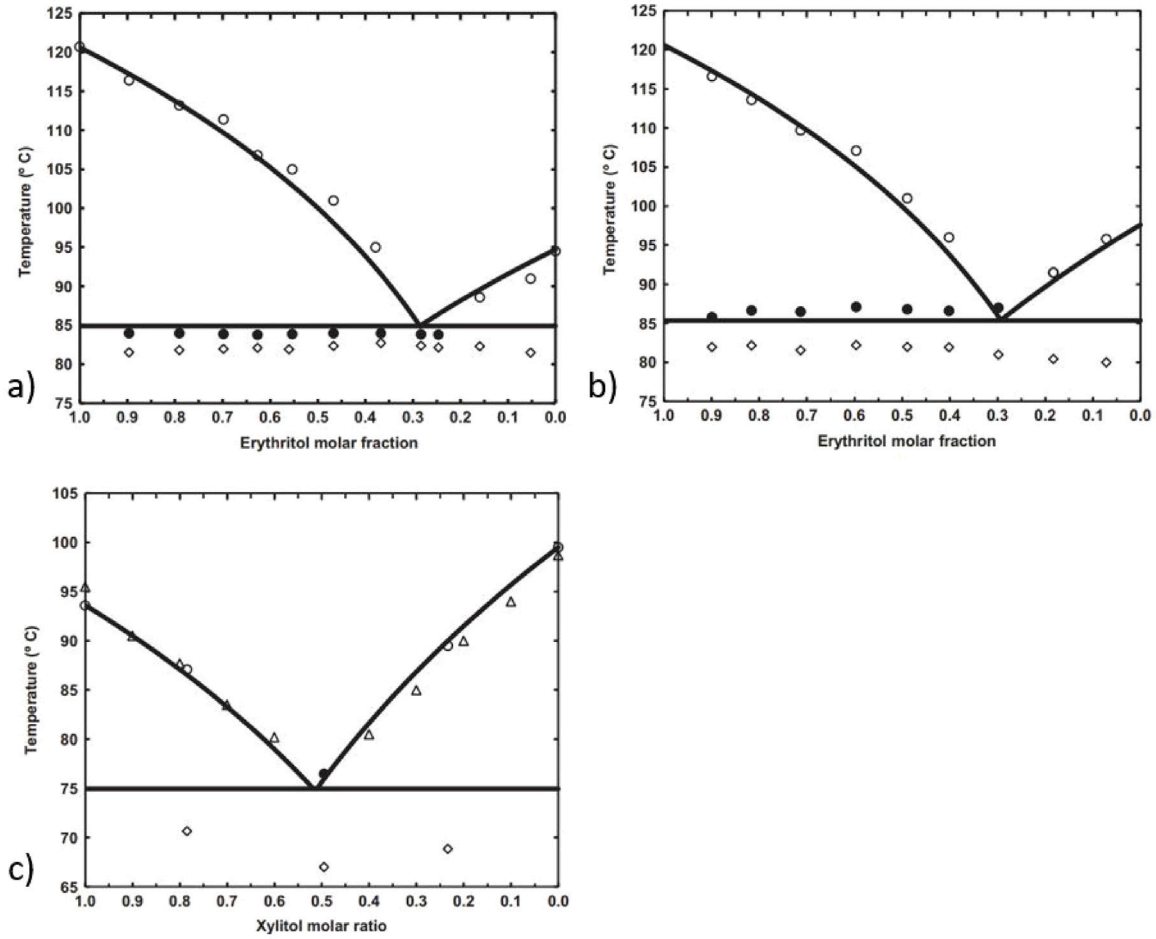

Fig. 17. Phase diagrams for (a) erythritol–xylitol, (b) erythritol–sorbitol, and (c) xylitol–sorbitol mixtures. Empty circles denote experimental inflection temperature of the 2nd endotherm (liquidus temperature); rhombi denote experimental onset temperature of the 1st endotherm; full circles represent experimental inflection temperature of 1st endotherm; lines represent predicted equilibrium temperatures using modified UNIFAC model [93].
Source: Image modified from Ref. [93].

3.2.2. Additivation of sugar alcohols

Seppä et al. [139] studied the introduction of various additives (SAT, salts, acids, water, alcohols) to enhance the rate of crystallization in subcooled xylitol, which exhibits subcooling of 70 °C and a crystallization rate of 0.7 ± 0.1 mm/h. The low value of the crystallization rate yields a reduced release of latent heat and, therefore, produces low discharging power. The tests were performed using sealed glass test tubes (diameter = 8 mm, height = 100 mm) filled with xylitol and various additives. After the xylitol melted, the tubes were placed in a constant-temperature water bath, and the speed of crystallization measured.

Some of the test tubes were placed in vertical position and the remaining in the horizontal position (insets in Fig. 20). The crystallization rates of xylitol with various additives in the vertical setup are summarized in Fig. 19. The effect of the methanol weight content on the crystallization rate of xylitol in both vertical and horizontal samples is illustrated in Fig. 20, which indicates that the crystallization rate in the vertical set up attained a maximum value that was 33 times higher than the one of pure xylitol. Furthermore, a gas gap existed above the xylitol in the horizontally oriented sample, and its crystallization rates attained values six times higher than those measured in the vertical setup.

In both the setups, the relaxation of the crystallized particles moving in the liquid zone enhanced the crystallization rate. Comparatively, the crystallized particles move more in the horizontal setup, thereby initiating the crystallization from the major crystallization zone (inset

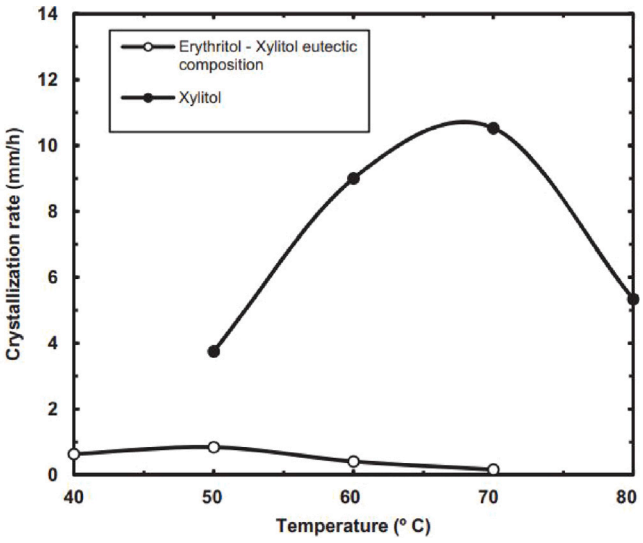

Fig. 18. Crystallization rate for pure xylitol and erythritol–xylitol eutectic composition.
Source: Image taken from Ref. [93].

Table 8
Thermophysical properties of eutectic mixtures of sugar alcohols.

	Molar ratios [–]	$T_{melting}$ [°C]	Heat content [kJ/kg]	Density liquid [kg/m^3]	Density solid [kg/m^3]	Specific heat solid [kJ/kg K]	Specific heat liquid [kJ/kg K]	Thermal conductivity solid [W/m K]	Thermal conductivity liquid [W/m K]	Reference
Threitol + Erythritol	76.6:25.4	78.6	248.8	–	–	–	–	–	–	[130]
Threitol + Arabinitol	63.9:36.1	72.8	236.5	–	–	–	–	–	–	[130]
Threitol + L-Arabitol	63.8:36.2	72.8	232.9	–	–	–	–	–	–	[130]
Threitol + L-Adonitol	62.9:37.1	72.3	230.7	–	–	–	–	–	–	[130]
Threitol + Xylitol	58.1:41.9	69.4	230.7	1490	–	1.38	–	–	–	[130]
Arabinitol + Adonitol	51.3:48.7	79.7	244.3	–	–	–	–	–	–	[130]
Arabinitol + Xylitol	43.4:56.6	77.6	246.3	–	–	1.30	–	0.6	–	[130]
Arabitol + Xylitol	41.7:58.3	78.4	242.4	–	–	–	–	–	–	[130]
Adonitol + Xylitol	44.4:55.6	77.1	240.2	–	–	–	–	–	–	[130]
L-arabitol + Erythritol	60:40	86	225	1312	1427	1.35	2.89	0.29	0.39	[95]
L-arabitol + Xylitol	44:56	77	243	1303	1480	0.88	2.18	0.40	0.36	[95]
Xylitol + Erythritol	64:36	82	270	1306	1467	1.02	2.29	0.38	0.418	[95]
Xylitol + Erythritol	75:25	77	–	–	–	–	–	0.39	0.40	[154]
Xylitol + Erythritol	75:25	83.9	248.7	–	–	–	–	–	–	[93]
D-Sorbitol + Erythritol	70:30	86.6	172.8	–	–	–	–	–	–	[93]
Xylitol + D-Sorbitol	52:48	74.6	169.6	–	–	–	–	–	–	[93]
Xylitol + D-Sorbitol	52:48	73.1	178.5	–	–	–	–	–	–	[90]
Xylitol + D-Sorbitol	52:48	74.4	183.4	–	–	–	–	–	–	[90]
Xylitol + Erythritol	75:25	82.9	201.4	–	–	–	–	–	–	[90]
Xylitol + Erythritol	75:25	83.5	233.3	–	–	–	–	–	–	[90]
D-sorbitol + Erythritol	70:30	86.1	173.6	–	–	–	–	–	–	[90]
D-sorbitol + Erythritol	70:30	86.5	175.8	–	–	–	–	–	–	[90]
Xylitol + D-Mannitol	96:4	91.7	166.8	–	–	–	–	–	–	[90]
Xylitol + D-Mannitol	96:4	91.3	157	–	–	–	–	–	–	[90]
Xylitol + D-Dulcitol	99:1	92.8	214.4	–	–	–	–	–	–	[90]
Xylitol + d-Dulcitol	99:1	92.9	226.9	–	–	–	–	–	–	[90]
Xylitol + Inositol	98:2	93.4	204.8	–	–	–	–	–	–	[90]
Xylitol + Inositol	98:2	93.4	230	–	–	–	–	–	–	[90]
M-Erythritol + D-Mannitol	87:23	114.4	322.8	–	–	–	–	–	–	[161]

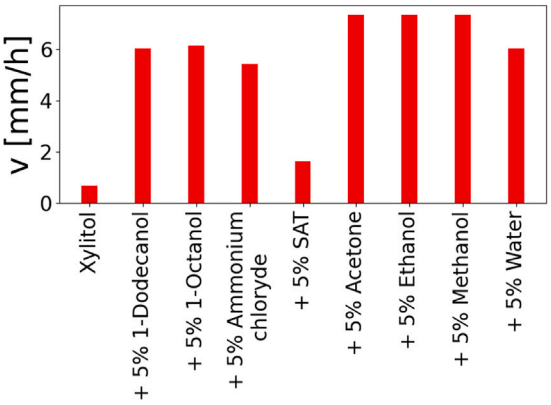

Fig. 19. Effect of various additives on crystallization rate of xylitol in vertical setup. v is the speed of the crystallization front [139].

in Fig. 20). This motion of the crystallized particles was caused by the lower density of the methanol as compared to that of xylitol. Thus, the effect of the additives is less evident in the vertical samples, because the movement of particles is hindered by the buoyant force.

In addition, the additives are used also to enhance the thermal performance of SAs. Pramothraj et al. [162] studied the addition of aluminum and copper microparticles to a D-Mannitol solution, and they reported an enhancement in both the decomposition temperatures and the enthalpy of fusion for weight contents up to 2% of additives. The addition of 2% weight content of Cu microparticles reduces the charging and discharging periods by 22% and 16%, respectively (refer to Fig. 21). In particular, copper microparticles delivered a greater enhancement than the aluminum microparticles. Several authors used graphene oxides nanosheets as additives to improve the thermal properties of erythritol [159]. The application of 1% in weight graphene oxides produced a two-fold increase in the overall thermal conductivity of the composite and enhanced the latent heat during crystallization from 187 to 225 kJ/kg. However, the degree of subcooling reduced by 16 °C (from 64 to 48 °C). The relative thermal conductivity enhancement and thermal conductivity value owing to the additivation of 1% in weight of various nanofillers in a solid erythritol matrix is comparatively presented in Fig. 22.

3.2.3. Prototypes

In the existing literature, certain studies have developed prototypes of TES containing SAs. Hirano and Takeuchi [147] experimentally evaluated a TES unit for supercooling. As depicted in Fig. 23, the cylindrical storage tank (stainless steel, 348 mm × 1745 mm) contained water and 96 cylindrical tubes of copper with a PCM (D-threitol) inside it. In particular, the tank was divided in a nucleation and TES section, wherein the nucleation section was in the bottom portion of the tank (1.3 L of water), and the TES section constituted the remaining portion (57.8 L of water). The study focused on the impact of the nucleation section on the spontaneous crystallization under thermal stratification. Excluding the nucleation section, the bottom portion of the tank exhibited a lower temperature owing to the thermal stratification when the system was maintained in a melted supercooled state. Within the nucleation section, an electric heater turns on in case the temperature is lower than the crystallization temperature (which is lower than the melting temperature owing to supercooling) to maintain the supercooled state in the bottom portion. This tank has been tested for a one- and three-days application. In both cases (especially in the second one), the system with the heater in the nucleation section delivered superior performance than that without it.

Another application is based on the patent developed by Guex et al. [152], where a reusable heat device containing xylitol is used as heat storage material.

3.2.4. Production processes

A majority of the eutectic mixtures of SAs are obtained by blending the melted single SAs using the stirring process and subsequently

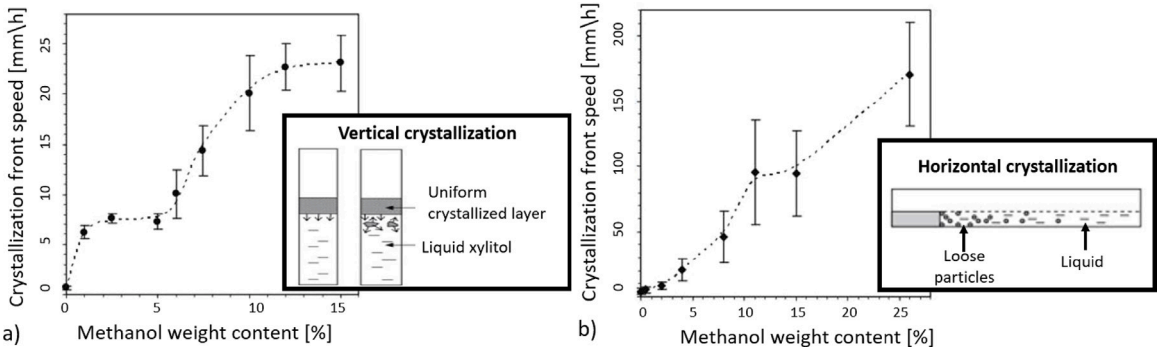

Fig. 20. Effect of methanol weight content on crystallization rate of xylitol under (a) vertical and (b) horizontal setup [139]. Layouts are presented in insets. *Source:* Images modified from Ref. [139].

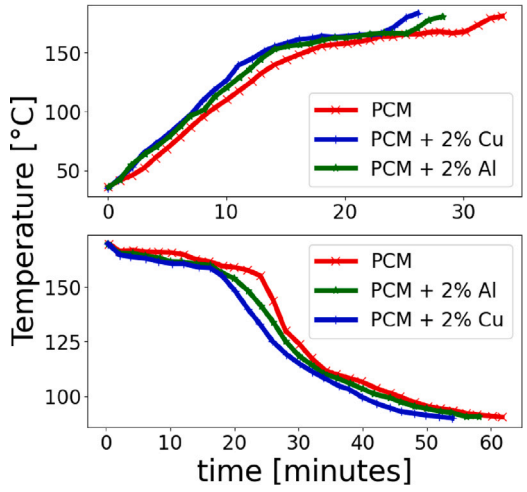

Fig. 21. (Top) Charging and (Bottom) discharging periods for pure D-Mannitol, D-Mannitol additivated with 2% wt. of Al and D-Mannitol additivated with 2% wt. of Cu [162].

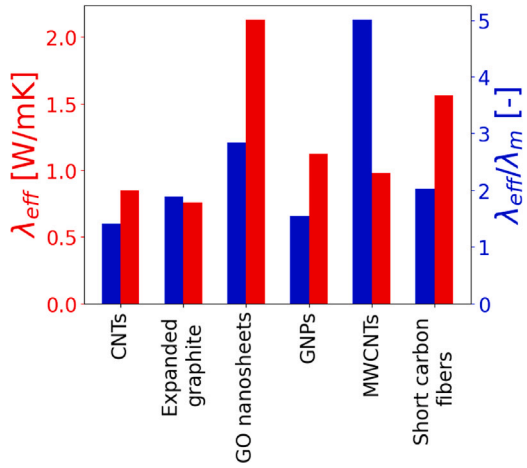

Fig. 22. Effect of 1% wt. of various nanofillers on thermal conductivity and thermal conductivity enhancement of erythritol-based nanocomposite in solid phase. λ_{eff} is the effective thermal conductivity of the composite, λ_m is the thermal conductivity of the matrix alone. Graphene oxide nanosheets (measured at 30 °C) [159], expanded graphite and CNTs [163], short carbon fibers (measured at 25 °C) [164], MWCNTs (measured at 50 °C) [165], and graphene nanoparticles [166] are shown.

cooling them [90]. In general, a powder grinding method is preferable for producing SA eutectic mixtures owing to the challenges posed by

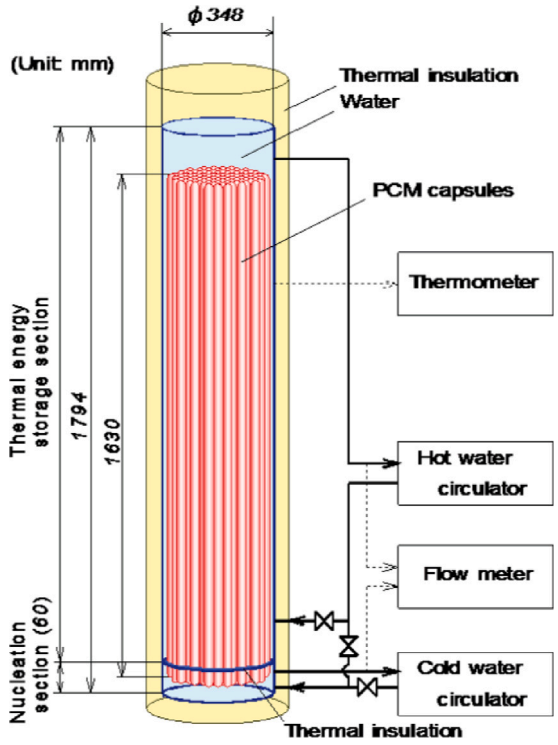

Fig. 23. Layout of TES tank containing SA used in Ref. [147].

crystallization and polymorphism [90,93]. This procedure involves the mixing of two components in the desired ratio and grinding them inside a mortar [130,154,161], which can be repeated several times by including additives such as diethylether to the solid mixture to facilitate mixing [93]. Moreover, a desiccation step can be performed to remove the moisture absorbed during the preparation of the mixture [154]. Ultimately, the obtained mixture is heated in an oven to obtain the eutectic mixture in the liquid form [161].

The introduction of nanoadditives to enhance the thermal conductivity of the composite is primarily performed by the procedures reported in Section 2. The additives as expanded graphite [161], graphite oxide nanosheets [159], aluminum and copper microparticles [162], and MWCNTs [167] can be added in the liquid phase of SAs (or SA eutectic mixtures) by means of stirring [159,161,162] and ultrasonication [159,167].

4. Solid–solid PCM

In classic solid-to-liquid PCMs (SL-PCMs), the crystalline arrangement in the solid phase becomes a disordered state in the liquid phase

after the bonds between the individual molecules are broken by the increased vibrational energy resulting from temperature rise. However, SL-PCMs pose structural limitations such as leakages in the liquid phase, a remarkable variation of volume between the two phases and possible phase segregation in heterogeneous mixtures.

Thus, in order to address these limitations, solid-to-solid PCMs (SS-PCMs) have recently garnered attention, especially for long-term applications. The SS-PCMs absorb and release thermal energy via phase transitions between a solid phase (crystalline, semicrystalline) and another solid phase (crystalline, semicrystalline or amorphous). During this transition, the material remains in the solid state and results in negligible phase segregation [168]. Moreover, as the transition occurs between the solid phases, the encapsulation of the material is not required.

There are two primary families of SS-PCMs. In the first family, the phase transition occurs between the two crystalline (or semicrystalline) structures during the absorption or release of heat [169]. In the second family, a soft segment, i.e., a structure with a lower melting temperature, is bonded to a hard segment, i.e., a secondary structure with higher melting temperature. Although the soft segment melts upon reaching the melting temperature, the overall structure is maintained in the solid phase owing to the bonds between the soft and hard segments that hinder the free movement of the melted structure [33].

The SS-PCMs can be classified as polymeric, inorganic, organometallic and organic nature [33].

4.1. Polymeric SS-PCMs

In polymeric SS-PCMs, the phase change component is bonded to a macromolecular backbone that hinders its movements. This bonding can be achieved via various processes such as side-chain grafting, as in polystyrene-g-PA, and crosslinking copolymerization, as in Melamine/Formaldehyde/Polyethyl Eneglycols (MFPEG) [33]. As compared to alternative SS-PCMs, polymeric SS-PCMs exhibit a lower latent heat, primarily owing to the lower amount of the phase change component and the restricted movement caused by the interactions between the two structures [33]. Moreover, they exhibit low thermal conductivity.

4.2. Inorganic SS-PCMs

Inorganic SS-PCMs require a combination of several solid-to-solid transformations (e.g., crystallographic structure and magnetic ones) to obtain adequately large latent heats. This multiple combination is allowed only in a limited number of material such as Fe [33].

4.3. Organometallic SS-PCMs

In organometallic SS-PCMs, organic and inorganic layers are bonded using ionic bonds in an alternate structure. The organic layer, i.e., a paraffinic chain, acts as soft segment, whereas the inorganic layer, i.e., perovskites, hinders the lateral movement maintaining the system in a solid phase. One of the most studied organometallic SS-PCM is $C_{10}Mn$ [170]. Basically, they exhibit the same limitation of polymeric SS-PCMs, such as low latent heat, as they follow the same mechanism. Nonetheless, the presence of the inorganic layer may increase the thermal conductivity by one order of magnitude compared to other SS-PCMs [33].

Table 9
Thermal conductivity of pentaerythritol as a function of temperature [184].

Thermal conductivity [W/m K]	Temperature [K]	Phase
0.66	303	α
0.53	453	α
0.23	483	γ
0.20	493	γ

4.4. Organic SS-PCMs

In organic SS-PCMs, the arrangement of molecules varies between crystalline phases with the absorption or release of heat [171]. Generally, SS-PCMs are polyalcohol organic compounds with a tetrahedral coordination (Plastic Crystals, PC), and they exhibit a solid-to-solid transition at a lower temperature than the solid-to-liquid transition. In addition, plastic crystals deliver the highest latent heat (110–300 J/g) and broadest melting temperature range (44–185 °C) among the SS-PCMs [33]. Moreover, the melting temperatures can be tuned using eutectic mixtures [169,172,173].

The plastic crystals are formed by spherical organic molecules with the centers of mass forming a crystalline lattice. In addition, they express a limited steric hindrance for reorientational processes owing to the spherical shape of the molecules [174]. Specifically, the molecules exhibit the preferred orientations at low temperatures because of the hydrogen bonding network between the hydroxyl groups and the repulsion between the methyl groups of adjacent molecules. Therefore, keeping the symmetric lattices of center of masses, the hydrogen bonds start to break owing to the random reorientation of the molecules with increased temperature [175,176]. At temperatures greater than the solid-to-solid phase transition, the hydrogen bonds cease to exist (or present in a limited number) and the intermolecular forces comprise only the van der Waals attractions [176]. Therefore, the crystalline structure modifies into an orientationally disordered phase during the phase transition to store a large amount of heat [177]. The mechanism of phase transition generated by breaking of the hydrogen bonding network results in the quasilinear dependence between the number of hydroxyl groups and the melting temperature of various plastic crystals. In particular, plastic crystals with less number of hydroxyl groups (e.g., neopentane) present a solid-to-solid transition at lower temperatures as compared to those with more hydroxyl groups (e.g., pentaerythritol) [176]. Materials that can be exploited as SS-PCMs are required to deliver high enthalpy of solid–solid latent heat, which amounts to a small enthalpy of fusion [178].

Overall, the most extensively studied plastic crystals include the pentaerythritol, pentaglycerine, neopentylglycol, and their eutectic mixtures [179–183].

Pentaerythritol (PE), $C(CH_2OH)_4$, displays a solid-to-solid phase transition with a latent heat of 280 kJ/kg at a temperature of 459 K [169,171,184,185]. The low-temperature phase, i.e., α phase, comprises a body-centered tetragonal structure, whereas the high-temperature phase, i.e., the γ phase, is an orientationally disordered face-centered cubic (FCC) structure [184]. According to molecular dynamics simulations of the solid-to-solid phase transition of PE [184], the different crystalline structures of each phase are responsible for their thermal conductivities. As listed in Table 9, the thermal conductivity in the α and γ phases linearly decreases with the temperature, whereas a sudden reduction of the transition temperature occurs owing to the variation of the crystalline structure. This reduction could be attributed to the breaking of the hydrogen bonding network in the γ phase since the H-bonds act as intermolecular bridges for the heat flux and increase the thermal conductivity of the material.

Pentaglycerine (PG), $CH_3C(CH_2OH)_3$ exhibits a latent heat of 172 kJ/kg at a transition temperature of 355 K [169]. In particular, the PG exists in a body-centered tetragonal structure in the low-temperature

Table 10
Relative thermal conductivity enhancements, reduction in enthalpies of transition, reduction in charging and discharging periods and reduction in subcooling caused by additivation of nanofillers in SS-PCMs. Negative values of enthalpy decrease means an increased latent heat stored due to the presence of nanofillers. PPMS: physical property measurement system, LFA: laser flash analysis.

Matrix	Filler	Filler content [%]	Enthalpy decrease [%]	λ_{eff}/λ_m [−]	Decrease in charging times [%]	Decrease in discharging times [%]	Subcooling decrease [%]	λ_{eff} measurements techniques	Ref.
Cellulose-graft-PEG copolymers	Expanded graphite	2 5 10	2 20 38	1.62 2.33 3.81	47.1 64.3 –	55.7 65.6 –	– – –	PPMS	[186]
Manganese based	Nano-gallium capsules	1 5	−2.22 −15.7	1.05 1.27	– –	– –	−11 7.12	LFA[a]	[187]
PG	GNPs	1 2 4	1.7 5 6.8	1.6 1.9 2.5	15.8 29 34.2	8.6 11.4 23	13.3 20 29.2	LFA	[188]
	Expanded graphite	1 2 4	1.1 1.86 3.8	2.8 3.72 4.1	30.5 41.60 52.8	32.4 32.30 62.1	8.6 10.78 9.78	LFA	[73]
PE	Low melting alloys	0.1 0.5	1.60 3.32	1.05 1.23	14.64 30.22	14.64 30.22	−0.5 0.8	LFA[a]	[189]
	Alumina nanoparticles	0.1 0.5 1	1.45 3.38 4.6	1.18 1.33 1.52	17.2 20.5 23	– – –	16.46 20.05 22.63	T-history	[190]
	Copper oxide nanoparticles	0.1 0.5	0.5 1.63	1.04 1.22	6.7 43.33	26.31 27	– –	LFA[a]	[191]
NPG	Copper oxide nanoparticles	0.5 1 3	3 4.7 9.6	1.16 2.5 4.08	14.2 22.83 33.9	20 29.6 38.3	– – –	LFA[a]	[192]

[a]Indicates that the measurement of the thermal diffusivity was performed, and the thermal conductivity was consequently computed numerically (measuring or estimating the density and the specific heat capacity).

phase, i.e., α phase, whereas it forms an orientationally disordered face-centered lattice in the high-temperature phase, i.e. the γ phase [176].

Neopentylglycol (NPG), $(CH_3)_2C(CH_2OH)_2$, having a phase-transition temperature of 317 K with a latent heat of 116 kJ/kg [169], represents one of the most promising plastic crystal for low-temperature TES applications. The low-temperature phase, i.e., α phase, includes a monoclinic phase, whereas the high-temperature phase, i.e., γ phase, includes an orientationally disordered face-centered lattice [176].

Moreover, binary and ternary mixtures of plastic crystals can be developed to adjust the transition temperatures and attain a broader temperature range of utilization [171,193–197].

4.5. Additivation in SS-PCMs

Similar to SL-PCMs, one of the major limitation of SS-PCMs pertains to their low thermal conductivity. As discussed in Section 2, similar procedures can be used to improve the thermal conductivity of SS-PCMs. In particular, nanoadditivation for SS-PCMs represents a more promising approach to enhance the thermal conductivity, because no liquid phase is involved and, thus, the drawback of reduced natural convection witnessed in SL-PCMs is insignificant in this context. The relative thermal conductivity enhancement, reduction in enthalpies, reduction in heat charging and discharging periods, reduction in subcooling and thermal conductivity measurement techniques reported in prior research for additivated SS-PCMs are summarized in Table 10. With regards to the reported measurements techniques, in the Laser Flash Analysis (LFA), whether thermal conductivity or diffusivity are measured, a light pulse heats up a surface of a sample and the resulting temperature variation as a function of time is measured on the rear face of the sample. Similarly, in the Physical Property Measurement System (PPMS), thermal conductivity is measured by monitoring the temperature change along a sample as a specific amount of heat passes through it. By contrast, in the T-history method, thermal properties of the PCM sample are measured by comparing them with those of a reference material. In the latter method, the sample, which consists of a long tube containing the PCM, is remarkably bigger than that of the other methods [198]: this feature is particularly suitable for measurement of the subcooling degree, as it is well known that the subcooling degree varies with the sample size. In the majority of the studies, the nanoadditivation results in a remarkable reduction of charging and discharging periods with a limited decrease in the enthalpy of transition.

Raj et al. [187] proposed an interesting approach, wherein nanogallium capsules (1 and 5% in weight content) were added to an organometallic SS-PCM, i.e., a manganese-based PCM. This addition (refer to Table 10) increased the thermal conductivity (up to 26.9%) and increased the latent heat (up to 15.7%), as the melting temperature of the filler is similar to the solid-to-solid phase transition temperature of the SS-PCM. Moreover, the coating of the nanogallium capsules can avoid leakages and maintain the overall system in a solid state.

The possibility of combining the advantages of SL-PCMs (as higher latent heat and lower cost) and those of SS-PCMs has been studied by Serrano et al. [194], wherein the SS-PCMs (PE, PG, and NPG, and their binary mixtures) were utilized as a supporting material for a SL-PCM (paraffin), thereby forming a shape-stabilized PCM. This coupled system can enhance the heat storage capacity of the SS-PCM and reduce its price while maintaining the advantages of solid-to-solid phase transition. The leakages in this storage system were avoided owing to the good wettability between the SS-PCMs and tested SL-PCMs. Overall, the studied systems exhibited higher heat storage capacities per unit of volume (up to 45%) and lower specific cost (up to 37%).

5. Conclusions

In this work, we have focused on selected PCMs and analyzed the reported procedures for enhancing and engineering their thermophysical properties by means of additives. In particular, we have reported on fillers with high thermal conductivity that have been extensively studied and discussed for thermal energy storage applications. Despite the intense scientific work in the literature, it is fair to claim that we still lack a comprehensive understanding on the optimal use of

fillers and additives to properly design PCMs with desired properties (i.e. sufficiently high effective thermal conductivity of the composite PCM). More specifically, as far as thermal properties are concerned, one important reason is related to the impact of the thermal resistances at the filler–matrix interface, which significantly limits heat transport within the material and whose control by current preparation procedures is still far from optimal. As a result, further improvements are required in terms of experiments, where new and more accurate techniques shall be developed to obtain more performing composites. Furthermore, the above effort should proceed hand-in-hand with more theoretical works as well, where an extensive analysis is to be performed to understand and better model the heat transport at complex matrix–filler and filler–filler interfaces.

In this work we have devoted a special effort on analyzing state-of-the-art knowledge on the use of additives and preparation procedure for enhancing liquid-to-solid PCMs subject to deep subcooling phenomena for long-term heat storage applications. It emerges that Sodium Acetate Trihydrate (SAT) and Sugar Alcohols are the most promising materials, although still plagued by serious issues related to inadequate thermophysical properties and stability. Despite the several reported attempts of material additivation, the use of the above materials in thermal energy storage applications is still characterized by a low technological maturity, thus requiring additional studies and experimentation.

In general, considerable room for improvement is foreseen in PCM-based long-term heat storage applications. Here, the discovery of new SS-PCMs, especially plastic crystals with outstanding solid-to-solid latent heat, appears a promising solution towards more stable and long-term heat storage systems where energy losses are significantly reduced. Interestingly, advances in the above field are expected to impact other fields as well. In particular, the application of barocaloric effects in these materials could be exploited to substitute the vapor-compression technologies with hydrocarbon refrigerants. However, the research in the above fields is still in its infancy and significant steps are required to resolve a number of relevant issues, i.e., enhancement of thermal conductivity, understanding the stable local minima to maintain the storage system in metastable conditions and the optimization of the barocaloric effect to exploit materials that require lower pressures.

Finally, in this work, we reviewed the state-of-the-art applications of additives for efficient heat storage and highlighted both the advantages and limitations of the current research topic to provide a perspective for improvements that may further advance the field of thermal energy storage.

Declaration of competing interest

The authors declare that they have no known competing financial interests or personal relationships that could have appeared to influence the work reported in this paper.

Acknowledgments

A.R. and E.C. acknowledge the financial support of the research contract PTR 2019/21 ENEA (Sviluppo di modelli per la caratterizzazione delle proprietà di scambio termico di PCM in presenza di additivi per il miglioramento dello scambio termico) funded by the Italian Ministry of Economic Development (MiSE). Support of the Italian National Project PRIN Heat transfer and Thermal Energy Storage Enhancement by Foams and Nanoparticles (2017F7KZWS) is also acknowledged. G.F., M.F and E.C. acknowledge useful discussions with Michele Bilancia.

References

[1] W. Liu, X. Zhang, J. Ji, Y. Wu, L. Liu, A review on thermal properties improvement of phase change materials and its combination with solar thermal energy storage, Energy Technol. 9 (2021).

[2] B. Mselle, G. Zsembinszki, E. Borri, D. Vé, L. Cabeza, Trends and future perspectives on the integration of phase change materials in heat exchangers, J. Energy Storage 38 (2021).

[3] P. De Angelis, M. Tuninetti, L. Bergamasco, L. Calianno, P. Asinari, F. Laio, M. Fasano, Data-driven appraisal of renewable energy potentials for sustainable freshwater production in africa, Renew. Sustain. Energy Rev. 149 (2021) 111414.

[4] IRENA, Innovation Outlook: Thermal Energy Storage, International Renewable Energy Agency, 2020.

[5] M. Fasano, L. Bergamasco, A. Lombardo, M. Zanini, E. Chiavazzo, P. Asinari, Water/ethanol and 13x zeolite pairs for long-term thermal energy storage at ambient pressure, Front. Energy Res. 7 (2019) 148.

[6] M. Fasano, G. Falciani, V. Brancato, V. Palomba, P. Asinari, E. Chiavazzo, A. Frazzica, Atomistic modelling of water transport and adsorption mechanisms in silicoaluminophosphate for thermal energy storage, Appl. Therm. Eng. 160 (2019) 114075.

[7] M. Fasano, D. Borri, A. Cardellini, M. Alberghini, M. Morciano, E. Chiavazzo, P. Asinari, Multiscale simulation approach to heat and mass transfer properties of nanostructured materials for sorption heat storage, Energy Procedia 126 (2017) 509–516.

[8] M. Fasano, D. Borri, E. Chiavazzo, P. Asinari, Protocols for atomistic modeling of water uptake into zeolite crystals for thermal storage and other applications, Appl. Therm. Eng. 101 (2016) 762–769.

[9] G. Trezza, L. Bergamasco, M. Fasano, E. Chiavazzo, Minimal crystallographic descriptors of sorption properties in hypothetical MOFs and role in sequential learning optimization, Comput. Mater. 8 (2022) 123.

[10] J.A. Noël, S. Kahwaji, L. Desgrosseilliers, D. Groulx, M.A. White, Chapter 13 - phase change materials, in: T.M. Letcher (Ed.), Storing Energy, Elsevier, Oxford, 2016, pp. 249–272.

[11] I. Dincer, On thermal energy storage systems and applications in buildings, Energy Build. 34 (2002) 377–388.

[12] A. Sharma, V. Tyagi, C. Chen, D. Buddhi, Review on thermal energy storage with phase change materials and applications, Renew. Sustain. Energy Rev. 13 (2009) 318–345.

[13] H. Benli, A. Durmuş, Performance analysis of a latent heat storage system with phase change material for new designed solar collectors in greenhouse heating, Sol. Energy 83 (2009) 2109–2119.

[14] A. Kü, Energy storage applications in greenhouses by means of phase change materials (pcms): a review, Renew. Energy 13 (1998) 89–103.

[15] A. Bologna, M. Fasano, L. Bergamasco, M. Morciano, F. Bersani, P. Asinari, L. Meucci, E. Chiavazzo, Techno-economic analysis of a solar thermal plant for large-scale water pasteurization, Appl. Sci. 10 (2020) 4771.

[16] T. Nomura, N. Okinaka, T. Akiyama, Waste heat transportation system, using phase change material (pcm) from steelworks to chemical plant, Resour. Conserv. Recy. 54 (2010) 1000–1006.

[17] A. Auckaili, M. Farid, A review on energy conservation in building applications with thermal storage by latent heat using phase change materials, Energy Convers. Manage. 45 (2004) 263–275.

[18] P. Schossig, H.-M. Henning, S. Gschwander, T. Haussmann, Micro-encapsulated phase-change materials integrated into construction materials, Sol. Energy Mater. Sol. Cells 89 (2005) 297–306, EuroSun2004.

[19] S. Mondal, Phase change materials for smart textiles – an overview, Appl. Therm. Eng. 28 (2008) 1536–1550.

[20] S. Wang, Y. Li, J. Hu, H. Tokura, Q. Song, Effect of phase-change material on energy consumption of intelligent thermal-protective clothing, Polym. Test. 25 (2006) 580–587.

[21] R. Kandasamy, X.-Q. Wang, A.S. Mujumdar, Application of phase change materials in thermal management of electronics, Appl. Therm. Eng. 27 (2007) 2822–2832.

[22] C. Alkan, E. Gü, S. Hiebler, Ömer F. Ensari, D. Kahraman, Polyurethanes as solid–solid phase change materials for thermal energy storage, Sol. Energy 86 (2012) 1761–1769.

[23] M. Kenisarin, K. Mahkamov, Solar energy storage using phase change materials, Renew. Sustain. Energy Rev. 11 (2007) 1913–1965.

[24] M. Neri, E. Chiavazzo, L. Mongibello, Numerical simulation and validation of commercial hot water tanks integrated with phase change material-based storage units, J. Energy Storage 32 (2020) 101938.

[25] Y. Yuan, N. Zhang, W. Tao, X. Cao, Y. He, Fatty acids as phase change materials: A review, Renew. Sustain. Energy Rev. 29 (2014) 482–498.

[26] G. Serale, Y. Cascone, A. Capozzoli, E. Fabrizio, M. Perino, Potentialities of a low temperature solar heating system based on slurry phase change materials (pcs), Energy Procedia 62 (2014) 355–363, 6th International Conference on Sustainability in Energy and Buildings, SEB-14.

[27] G. Englmair, Y. Jiang, M. Dannemand, C. Moser, H. Schranzhofer, S. Furbo, J. Fan, Crystallization by local cooling of supercooled sodium acetate trihydrate composites for long-term heat storage, Energy Build. 180 (2018) 159–171.

[28] K. Seo, S. Suzuki, T. Kinoshita, I. Hirasawa, Effect of ultrasonic irradiation on the crystallization of sodium acetate trihydrate utilized as heat storage material, Chem. Eng. Technol. 35 (2012) 1013–1016.

[29] J.B. Johansen, M. Dannemand, W. Kong, J. Fan, J. Dragsted, S. Furbo, Thermal conductivity enhancement of sodium acetate trihydrate by adding graphite powder and the effect on stability of supercooling, Energy Procedia 70 (2015) 249–256, International Conference on Solar Heating and Cooling for Buildings and Industry, SHC 2014.
[30] G. Zhou, Y. Xiang, Experimental investigations on stable supercooling performance of sodium acetate trihydrate pcm for thermal storage, Sol. Energy 155 (2017) 1261–1272.
[31] G. Zhou, M. Zhu, Y. Xiang, Effect of percussion vibration on solidification of supercooled salt hydrate pcm in thermal storage unit, Renew. Energy 126 (2018) 537–544.
[32] H.W. Ryu, S.W. Woo, B.C. Shin, S.D. Kim, Prevention of supercooling and stabilization of inorganic salt hydrates as latent heat storage materials, Sol. Energy Mater. Sol. Cells 27 (1992) 161–172, Special Issue on Heat Storage Materials.
[33] A. Fallahi, G. Guldentops, M. Tao, S. Granados-Focil, S. Van Dessel, Review on solid–solid phase change materials for thermal energy storage: Molecular structure and thermal properties, Appl. Therm. Eng. 127 (2017) 1427–1441.
[34] L. Bergamasco, M. Alberghini, M. Fasano, A. Cardellini, E. Chiavazzo, P. Asinari, Mesoscopic moment equations for heat conduction: characteristic features and slow–fast mode decomposition, Entropy 20 (2018) 126.
[35] B. Zalba, J.M. Marın, L.F. Cabeza, H. Mehling, Review on thermal energy storage with phase change: materials, heat transfer analysis and applications, Appl. Therm. Eng. 23 (2003) 251–283.
[36] N.S. Dhaidan, S.A. Kokz, F.L. Rashid, A.K. Hussein, O. Younis, F.N. Al-Mousawi, Review of solidification of phase change materials dispersed with nanoparticles in different containers, J. Energy Storage 51 (2022) 104271.
[37] K.Y. Leong, M.R. Abdul Rahman, B.A. Gurunathan, Nano-enhanced phase change materials: A review of thermo-physical properties, applications and challenges, J. Energy Storage 21 (2019) 18–31.
[38] E.J. D'Oliveira, S.C.C. Pereira, D. Groulx, U. Azimov, Thermophysical properties of nano-enhanced phase change materials for domestic heating applications, J. Energy Storage 46 (2022) 103794.
[39] R. Kumar, A. Mitra, T. Srinivas, Role of nano-additives in the thermal management of lithium-ion batteries: A review, J. Energy Storage 48 (2022) 104059.
[40] B.M.S. Punniakodi, R. Senthil, Recent developments in nano-enhanced phase change materials for solar thermal storage, Sol. Energy Mater. Sol. Cells 238 (2022) 111629.
[41] Y. Lin, Y. Jia, G. Alva, G. Fang, Review on thermal conductivity enhancement, thermal properties and applications of phase change materials in thermal energy storage, Renew. Sustain. Energy Rev. 82 (2018) 2730–2742.
[42] S. Wu, T. Yan, Z. Kuai, W. Pan, Thermal conductivity enhancement on phase change materials for thermal energy storage: A review, Energy Storage Mater. 25 (2020) 251–295.
[43] I. Shamseddine, F. Pennec, P. Biwole, F. Fardoun, Supercooling of phase change materials: A review, Renew. Sustain. Energy Rev. 158 (2022) 112172.
[44] L. Que, X. Zhang, J. Ji, L. Gao, W. Xie, L. Liu, X. Ding, Numerical simulation and experimental research progress of phase change hysteresis: A review, Energy Build. 253 (2021) 111402.
[45] A. Yadav, A. Verma, A. Kumar, H. Dashmana, A. Kumar, P. Bhatnagar, V. Jain, Recent advances on enhanced thermal conduction in phase change materials using carbon nanomaterials, J. Energy Storage 43 (2021) 103173.
[46] A. Al-Ahmed, M.A.J. Mazumder, B. Salhi, A. Sari, M. Afzaal, F.A. Al-Sulaiman, Effects of carbon-based fillers on thermal properties of fatty acids and their eutectics as phase change materials used for thermal energy storage: A review, J. Energy Storage 35 (2021) 102329.
[47] B. Buonomo, D. Ercole, O. Manca, S. Nardini, Numerical analysis on a latent thermal energy storage system with phase change materials and aluminum foam, Heat Transfer Eng. 41 (2020) 1075–1084.
[48] A. Ribezzo, M. Fasano, L. Bergamasco, L. Mongibello, E. Chiavazzo, Multi-scale numerical modelling for predicting thermo-physical properties of phase-change nanocomposites for cooling energy storage, Tecnica Italiana-Ital. J. Eng. Sci. 65 (2021) 201–204.
[49] Z. Sunxi, Z. Xuelai, L. Sheng, L. Yuyang, X. Xiaofeng, Performance study on expand graphite/organic composite phase change material for cold thermal energy storage, Energy Procedia 158 (2019) 5305–5310, Innovative Solutions for Energy Transitions.
[50] R. Al-Shannaq, M.M. Farid, A novel graphite-pcm composite sphere with enhanced thermo-physical properties, Appl. Therm. Eng. 142 (2018) 401–409.
[51] R. Al-Shannaq, B. Young, M. Farid, Cold energy storage in a packed bed of novel graphite/pcm composite spheres, Energy 171 (2019) 296–305.
[52] T. Xiong, K.W. Shah, Chapter 26 - nanomaterials for enhancement of thermal energy storage in building applications, in: C. Mustansar Hussain (Ed.), Handbook of Functionalized Nanomaterials for Industrial Applications, Micro and Nano Technologies, Elsevier, 2020, pp. 829–864.
[53] R. Srivastava, M. Fasano, S. Mohammad Nejad, H. Chávez Thielemann, E. Chiavazzo, P. Asinari, 3 Modeling carbon-based smart materials, pp. 33–80.
[54] A. Marconnet, M. Panzer, K. Goodson, Thermal conduction phenomena in carbon nanotubes and related nanostructured materials, Rev. Modern Phys. 85 (2013).
[55] S.Y. Kim, Y.J. Noh, J. Yu, Thermal conductivity of graphene nanoplatelets filled composites fabricated by solvent-free processing for the excellent filler dispersion and a theoretical approach for the composites containing the geometrized fillers, Composites A 69 (2015) 219–225.
[56] M. Fasano, M. Bozorg Bigdeli, M.R. Vaziri Sereshk, E. Chiavazzo, P. Asinari, Thermal transmittance of carbon nanotube networks: Guidelines for novel thermal storage systems and polymeric material of thermal interest, Renew. Sustain. Energy Rev. 41 (2015) 1028–1036.
[57] R.K. Abu Al-Rub, A.I. Ashour, B.M. Tyson, On the aspect ratio effect of multi-walled carbon nanotube reinforcements on the mechanical properties of cementitious nanocomposites, Constr. Build. Mater. 35 (2012) 647–655.
[58] Y. Cui, C. Liu, S. Hu, X. Yu, The experimental exploration of carbon nanofiber and carbon nanotube additives on thermal behavior of phase change materials, Sol. Energy Mater. Sol. Cells 95 (2011) 1208–1212.
[59] R.P. Singh, J.Y. Sze, S.C. Kaushik, D. Rakshit, A. Romagnoli, Thermal performance enhancement of eutectic pcm laden with functionalised graphene nanoplatelets for an efficient solar absorption cooling storage system, J. Energy Storage 33 (2021) 102092.
[60] L.-W. Fan, X. Fang, X. Wang, Y. Zeng, Y.-Q. Xiao, Z.-T. Yu, X. Xu, Y.-C. Hu, K.-F. Cen, Effects of various carbon nanofillers on the thermal conductivity and energy storage properties of paraffin-based nanocomposite phase change materials, Appl. Energy 110 (2013) 163–172.
[61] B.N.J. Persson, Thermal interface resistance: cross-over from nanoscale to macroscale, J. Phys.: Condens. Matter 26 (2013) 015009.
[62] M.M. Sadeghi, I. Jo, L. Shi, Phonon-interface scattering in multilayer graphene on an amorphous support, Proc. Natl. Acad. Sci. 110 (2013) 16321–16326.
[63] S. Mohammad Nejad, R. Srivastava, F.M. Bellussi, H. Chávez Thielemann, P. Asinari, M. Fasano, Nanoscale thermal properties of carbon nanotubes/epoxy composites by atomistic simulations, Int. J. Therm. Sci. 159 (2021) 106588.
[64] E. Chiavazzo, P. Asinari, Enhancing surface heat transfer by carbon nanofins: towards an alternative to nanofluids? Nanoscale Res. Lett. 6 (2011).
[65] A.S. Tascini, J. Armstrong, E. Chiavazzo, M. Fasano, P. Asinari, F. Bresme, Thermal transport across nanoparticle–fluid interfaces: the interplay of interfacial curvature and nanoparticle–fluid interactions, Phys. Chem. Chem. Phys. 19 (2017) 3244–3253.
[66] V. Kumaresan, R. Velraj, S.K. Das, The effect of carbon nanotubes in enhancing the thermal transport properties of pcm during solidification, Heat Mass Transf. 48 (2012) 1345–1355.
[67] R.P. Singh, J.Y. Sze, S.C. Kaushik, D. Rakshit, A. Romagnoli, Thermal performance enhancement of eutectic pcm laden with functionalised graphene nanoplatelets for an efficient solar absorption cooling storage system, J. Energy Storage 33 (2021) 102092.
[68] L. He, H. Wang, H. Zhu, Y. Gu, X. Li, X. Mao, Thermal properties of peg/graphene nanoplatelets (gnps) composite phase change materials with enhanced thermal conductivity and photo-thermal performance, Appl. Sci. 8 (2018) 2613.
[69] E. Chiavazzo, P. Asinari, Reconstruction and modeling of 3d percolation networks of carbon fillers in a polymer matrix, Int. J. Therm. Sci. 49 (2010) 2272–2281.
[70] R.J. Warzoha, A.S. Fleischer, Effect of graphene layer thickness and mechanical compliance on interfacial heat flow and thermal conduction in solid–liquid phase change materials, ACS Appl. Mater. Interfaces 6 (2014) 12868–12876, PMID: 24983698.
[71] G. He, X. Tian, Y. Dai, X. Li, C. Lin, Z. Yang, S. Liu, Bioinspired interfacial engineering of polymer based energetic composites towards superior thermal conductivity via reducing thermal resistance, Appl. Surf. Sci. 493 (2019) 679–690.
[72] A. Rybak, Processing Influence on Thermal Conductivity of Polymer Nanocomposites, pp. 463–487.
[73] N. Zhang, Y. Song, Y. Du, Y. Yuan, G. Xiao, Y. Gui, A novel solid–solid phase change material: Pentaglycerine/expanded graphite composite pcms, Adv. Energy Mater. 20 (2018) 1800237.
[74] A. Ohayon-Lavi, A. Lavi, A. Alatawna, E. Ruse, G. Ziskind, O. Regev, Graphite-based shape-stabilized composites for phase change material applications, Renew. Energy 167 (2021) 580–590.
[75] S. Harikrishnan, S. Magesh, S. Kalaiselvam, Preparation and thermal energy storage behaviour of stearic acid–tio2 nanofluids as a phase change material for solar heating systems, Thermochim. Acta 565 (2013) 137–145.
[76] Z. Sunxi, Z. Xuelai, L. Sheng, L. Yuyang, X. Xiaofeng, Performance study on expand graphite/organic composite phase change material for cold thermal energy storage, Energy Procedia 158 (2019) 5305–5310, Innovative Solutions for Energy Transitions.
[77] A.K. Mishra, B.B. Lahiri, J. Philip, Effect of surface functionalization and physical properties of nanoinclusions on thermal conductivity enhancement in an organic phase change material, ACS Omega 3 (2018) 9487–9504.
[78] A. Safari, R. Saidur, F. Sulaiman, Y. Xu, J. Dong, A review on supercooling of phase change materials in thermal energy storage systems, Renew. Sustain. Energy Rev. 70 (2017) 905–919.
[79] N. Kumar, J. Hirschey, T.J. LaClair, K.R. Gluesenkamp, S. Graham, Review of stability and thermal conductivity enhancements for salt hydrates, J. Energy Storage 24 (2019) 100794.

[80] A. Sharma, V.V. Tyagi, C. Chen, D. Buddhi, Review on thermal energy storage with phase change materials and applications, Renew. Sustain. Energy Rev. 13 (2009) 318–345.

[81] M.H. Zahir, S.A. Mohamed, R. Saidur, F.A. Al-Sulaiman, Supercooling of phase-change materials and the techniques used to mitigate the phenomenon, Appl. Energy 240 (2019) 793–817.

[82] P.G. Debenedetti, Metastable Liquids: Concepts and Principles, Princeton University Press, 1996.

[83] E.B. Moore, V. Molinero, Structural transformation in supercooled water controls the crystallization rate of ice, Nature 479 (2011) 506.

[84] L. Yuan, Q. Ge, H. Fu, G. Jiang, Z. Yu, Q. Zheng, Y. Lv, J. Zhao, J. Yu, Sodium acetate trihydrate–crystallization inhibitor system for seasonal latent heat storage, J. Energy Eng. 144 (2018) 04018022.

[85] G.A. Lane, Phase change materials for energy storage nucleation to prevent supercooling, Sol. Energy Mater. Sol. Cells 27 (1992) 135–160.

[86] X. Zhang, J. Niu, S. Zhang, J.-Y. Wu, Pcm in water emulsions: Supercooling reduction effects of nano-additives, viscosity effects of surfactants and stability, Adv. Energy Mater. 17 (2015) 181–188.

[87] D. Lee, D. Kim, C. Kang, Effects of nanostructure additives on supercooling and freezing of distilled water, Int. J. Air-Cond. Refrigeration 28 (2020) 1–9.

[88] C.R. Raj, S. Suresh, R. Bhavsar, V.K. Singh, A.S. Reddy, A. Upadhyay, Manganese-based layered perovskite solid–solid phase change material: Synthesis, characterization and thermal stability study, Mech. Mater. 135 (2019) 88–97.

[89] Y. Nakamura, Y. Sakai, M. Azuma, S.-i. Ohkoshi, Long-term heat-storage ceramics absorbing thermal energy from hot water, Sci. Adv. 6 (2020).

[90] X.-F. Shao, C. Wang, Y.-J. Yang, B. Feng, Z.-Q. Zhu, W.-J. Wang, Y. Zeng, L.-W. Fan, Screening of sugar alcohols and their binary eutectic mixtures as phase change materials for low-to-medium temperature latent heat storage. *i*: Non-isothermal melting and crystallization behaviors, Energy 160 (2018) 1078–1090.

[91] M. Dannemand, W. Kong, J. Fan, J.B. Johansen, S. Furbo, Laboratory test of a prototype heat storage module based on stable supercooling of sodium acetate trihydrate, Energy Procedia 70 (2015) 172–181.

[92] M. Dannemand, J. Dragsted, J. Fan, J.B. Johansen, W. Kong, S. Furbo, Experimental investigations on prototype heat storage units utilizing stable supercooling of sodium acetate trihydrate mixtures, Appl. Energy 169 (2016) 72–80.

[93] G. Diarce, I. Gandarias, A. Campos-Celador, A. Garcia-Romero, U. Griesser, Eutectic mixtures of sugar alcohols for thermal energy storage in the 50–90 °C temperature range, Sol. Energy Mater. Sol. Cells 134 (2015) 215–226.

[94] S. Hö, A. Kö, D. Brü, Thermophysical characterization of MgCl2 6H2O, Xylitol and Erythritol as Phase Change Materials (PCM) for Latent Heat Thermal Energy Storage (LHTES), Materials (2017).

[95] E.P. del Barrio, A. Godin, M. Duquesne, J. Daranlot, J. Jolly, W. Alshaer, T. Kouadio, A. Sommier, Characterization of different sugar alcohols as phase change materials for thermal energy storage applications, Sol. Energy Mater. Sol. Cells 159 (2017) 560–569.

[96] M.A.R. Ibrahim Dincer, Thermal Energy Storage: Systems and Applications, second ed., Princeton University Press, 2010.

[97] K.K. Meisingset, F. Grønvold, Thermodynamic properties and phase transitions of salt hydrates between 270 and 400 K III. CH3CO2Na · 3H2O, CH3CO2Li · 2H2O, and (CH3CO2) 2Mg · 4H2O, J. Chem. Thermodyn. 16 (1984) 523–536.

[98] N. Araki, M. Futamura, A. Makino, H. Shibata, Measurements of thermophysical properties of sodium acetate hydrate, Int. J. Thermophys. 16 (1995) 1455–1466.

[99] A. Kaizawa, N. Maruoka, A. Kawai, H. Kamano, T. Jozuka, T. Senda, T. Akiyama, Thermophysical and heat transfer properties of phase change material candidate for waste heat transportation system, Heat Mass Transf. 44 (2008) 763–769.

[100] Y. Wang, K. Yu, H. Peng, X. Ling, Preparation and thermal properties of sodium acetate trihydrate as a novel phase change material for energy storage, Energy 167 (2019) 269–274.

[101] Q. Xiao, M. Zhang, J. Fan, L. Li, T. Xu, W. Yuan, Thermal conductivity enhancement of hydrated salt phase change materials employing copper foam as the supporting material, Sol. Energy Mater. Sol. Cells 199 (2019) 91–98.

[102] J. Liu, C. Zhu, W. Liang, Y. Li, H. Bai, Q. Guo, C. Wang, Experimental investigation on micro-scale phase change material based on sodium acetate trihydrate for thermal storage, Sol. Energy 193 (2019) 413–421.

[103] M. Li, Z. Lin, Y. Sun, F. Wu, T. Xu, H. Wu, X. Zhou, D. Wang, Y. Liu, Preparation and characterizations of a novel temperature-tuned phase change material based on sodium acetate trihydrate for improved performance of heat pump systems, Renew. Energy 157 (2020) 670–677.

[104] X. Jin, F. Wu, T. Xu, G. Huang, H. Wu, X. Zhou, D. Wang, Y. Liu, A.C. Lai, Experimental investigation of the novel melting point modified phase–change material for heat pump latent heat thermal energy storage application, Energy 216 (2021) 119191.

[105] Y. He, Y. Song, Y. Yuan, L. Yang, N. Zhang, Experimental investigation on the supercooling and heat conduction of sodium acetate trihydrate/copper foam/YSZ composite phase change material, J. Therm. Anal. Calorim. 143 (2021) 3275–3284.

[106] Z. Zhang, Z. Duan, D. Chen, Y. Xie, X. Cao, J. Wang, Sodium acetate trihydrate-based composite phase change material with enhanced thermal performance for energy storage, J. Energy Storage 34 (2021) 102186.

[107] use of cellulose nanofibril (cnf)/silver nanoparticles (agnps) composite in salt hydrate phase change material for efficient thermal energy storage.

[108] S. Guillén-Lambea, M. Carvalho, M. Delgado, A. Lazaro, Sustainable enhancement of district heating and cooling configurations by combining thermal energy storage and life cycle assessment, Clean Technol. Environ. Policy (2020) 1–11.

[109] Z. Shen, S. Kwon, H.L. Lee, M. Toivakka, K. Oh, Enhanced thermal energy storage performance of salt hydrate phase change material: Effect of cellulose nanofibril and graphene nanoplatelet, Sol. Energy Mater. Sol. Cells 225 (2021) 111028.

[110] L. Wei, K. Ohsasa, Supercooling and solidification behavior of phase change material, ISIJ Int. 50 (2010) 1265–1269.

[111] R. Rybár, M. Beer, M. Kalavskỳ, Development of heat accumulation unit based on heterogeneous structure of MF/PCM for cogeneration units, J. Energy Storage 21 (2019) 72–77.

[112] M. Dannemand, J.B. Johansen, W. Kong, S. Furbo, Experimental investigations on cylindrical latent heat storage units with sodium acetate trihydrate composites utilizing supercooling, Appl. Energy 177 (2016) 591–601.

[113] M. Dannemand, J.B. Johansen, S. Furbo, Solidification behavior and thermal conductivity of bulk sodium acetate trihydrate composites with thickening agents and graphite, Sol. Energy Mater. Sol. Cells 145 (2016) 287–295.

[114] G. Englmair, C. Moser, H. Schranzhofer, J. Fan, S. Furbo, A solar combi-system utilizing stable supercooling of sodium acetate trihydrate for heat storage: Numerical performance investigation, Appl. Energy 242 (2019) 1108–1120.

[115] G. Englmair, S. Furbo, M. Dannemand, J. Fan, Experimental investigation of a tank-in-tank heat storage unit utilizing stable supercooling of sodium acetate trihydrate, Appl. Therm. Eng. 167 (2020) 114709.

[116] G. Englmair, W. Kong, J.B. Berg, S. Furbo, J. Fan, Demonstration of a solar combi-system utilizing stable supercooling of sodium acetate trihydrate for heat storage, Appl. Therm. Eng. 166 (2020) 114647.

[117] G. Wang, M. Dannemand, C. Xu, G. Englmair, S. Furbo, J. Fan, Thermal characteristics of a long-term heat storage unit with sodium acetate trihydrate, Appl. Therm. Eng. 187 (2021) 116563.

[118] Y. Ouchi, S. Someya, T. Munakata, H. Ito, Visualization of the phase change behavior of sodium acetate trihydrate for latent heat storage, Appl. Therm. Eng. 91 (2015) 547–555.

[119] A. Abhat, Low temperature latent heat thermal energy storage: heat storage materials, Sol. Energy 30 (1983) 313–332.

[120] B. Sandnes, J. Rekstad, Supercooling salt hydrates: Stored enthalpy as a function of temperature, Sol. Energy 80 (2006) 616–625.

[121] T. Wada, R. Yamamoto, Y. Matsuo, Heat storage capacity of sodium acetate trihydrate during thermal cycling, Sol. Energy 33 (1984) 373–375.

[122] Y.R. Li, T. Inagaki, H. Kashiwa, Thermo-physical properties of phase change materials and those natural convection heat transfer in a horizontal enclosed rectangular container, in: Applied Mechanics and Materials, Vol. 620, Trans Tech Publ, pp. 468–471.

[123] N. Beaupere, U. Soupremanien, L. Zalewski, Influence of water addition on the latent heat degradation of sodium acetate trihydrate, Appl. Sci. 11 (2021) 484.

[124] W. Kong, M. Dannemand, J.B. Johansen, J. Fan, J. Dragsted, G. Englmair, S. Furbo, Experimental investigations on heat content of supercooled sodium acetate trihydrate by a simple heat loss method, Sol. Energy 139 (2016) 249–257.

[125] W. Kong, M. Dannemand, J. Berg, J. Fan, J. Dragsted, S. Furbo, Ageing stability of sodium acetate trihydrate with and without additives for seasonal heat storage, pp. 1–10.

[126] J. Fan, S. Furbo, E. Andersen, Z. Chen, B. Perers, M. Dannemand, Thermal behavior of a heat exchanger module for seasonal heat storage, Energy Procedia 30 (2012) 244–254.

[127] Private communication. F., Froese used to work in the company LaTherm, 2018.

[128] M. Dannemand, J.M. Schultz, J.B. Johansen, S. Furbo, Long term thermal energy storage with stable supercooled sodium acetate trihydrate, Appl. Therm. Eng. 91 (2015) 671–678.

[129] W. Kong, M. Dannemand, J. Brinkø Berg, J. Fan, G. Englmair, J. Dragsted, S. Furbo, Experimental investigations on phase separation for different heights of sodium acetate water mixtures under different conditions, Appl. Therm. Eng. 148 (2019) 796–805.

[130] E. Palomo Del Barrio, R. Cadoret, J. Daranlot, F. Achchaq, New sugar alcohols mixtures for long-term thermal energy storage applications at temperatures between 70 °C and 100 °C, Sol. Energy Mater. Sol. Cells 155 (2016) 454–468.

[131] N.R. Jankowski, F.P. McCluskey, A review of phase change materials for vehicle component thermal buffering, Appl. Energy 113 (2014) 1525–1561.

[132] P. Collins, Dictionary of Carbohydrates, second ed., Chapman and Hall/CRC, 2005.

[133] W. Wang, S. Guo, H. Li, J. Yan, J. Zhao, X. Li, J. Ding, Experimental study on the direct/indirect contact energy storage container in mobilized thermal energy system (M-TES), Appl. Energy 119 (2014) 181–189.

[134] F. Agyenim, P. Eames, M. Smyth, Experimental study on the melting and solidification behaviour of a medium temperature phase change storage material (Erythritol) system augmented with fins to power a LiBr/H2O absorption cooling system, Renew. Energy 36 (2011) 108–117.
[135] J. Shon, H. Kim, K. Lee, Improved heat storage rate for an automobile coolant waste heat recovery system using phase-change material in a fin–tube heat exchanger, Appl. Energy 113 (2014) 680–689.
[136] B. Tong, Z.C. Tan, J.N. Zhang, S.X. Wang, Thermodynamic investigation of several natural polyols, J. Therm. Anal. Calorim. 95 (2009) 469–475.
[137] A. Shukla, D. Buddhi, R. Sawhney, Thermal cycling test of few selected inorganic and organic phase change materials, Renew. Energy 33 (2008) 2606–2614.
[138] A. Sari, R. Eroglu, A. Biçer, A. Karaipekli, Synthesis and thermal energy storage properties of erythritol tetrastearate and erythritol tetrapalmitate, Chem. Eng. Technol. 34 (2011) 87–92.
[139] A. Seppä, A. Merilä, L. Wikströ, P. Kauranen, The effect of additives on the speed of the crystallization front of xylitol with various degrees of supercooling, Exp. Therm Fluid Sci. 34 (2010) 523–527.
[140] A. Solé, H. Neumann, S. Niedermaier, I. Martorell, P. Schossig, L.F. Cabeza, Stability of sugar alcohols as PCM for thermal energy storage, Sol. Energy Mater. Sol. Cells 126 (2014) 125–134.
[141] G. Kumaresan, R. Velraj, S. Iniyan, Thermal analysis of d-mannitol for use as phase change material for latent heat storage, J. Appl. Sci. 11 (2011) 3044–3048.
[142] C. Barreneche, A. Gil, F. Sheth, A. Iné, L.F. Cabeza, Effect of d-mannitol polymorphism in its thermal energy storage capacity when it is used as PCM, Sol. Energy 94 (2013) 344–351.
[143] A. Mojiri, N. Grbac, B. Bourke, G. Rosengarten, D-mannitol for medium temperature thermal energy storage, Sol. Energy Mater. Sol. Cells 176 (2018) 150–156.
[144] M.-M. Rodríguez-García, R. Bayón, E. Rojas, Stability of d-mannitol upon melting/freezing cycles under controlled inert atmosphere, Energy Procedia 91 (2016) 218–225, Proceedings of the 4th International Conference on Solar Heating and Cooling for Buildings and Industry (SHC 2015).
[145] H. Neumann, S. Niedermaier, S. Gschwander, P. Schossig, Cycling stability of d-mannitol when used as phase change material for thermal storage applications, Thermochim. Acta 660 (2018) 134–143.
[146] W.C. Winegard, S. Majka, B.M. Thall, B. Chalmers, Eutectic solidification in metals, Can. J. Chem. 29 (1951) 320–327.
[147] S. Hirano, H. Takeuchi, Characteristic of reheating operation in supercooled thermal energy storage unit for hot water supply or space heating, Energy Procedia 57 (2014) 3140–3149.
[148] H. Hidaka, M. Yamazaki, M. Yabe, H. Kakiuchi, E.P. Ona, Y. Kojima, H. Matsuda, Evaluation of fundamental characteristics of d-threitol as phase change material at high temperature, in: Asian Pacific Confederation of Chemical Engineering Congress Program and Abstracts Asian Pacific Confederation of Chemical Engineers Congress Program and Abstracts, The Society of Chemical Engineers, Japan, pp. 535–535.
[149] L. Carpentier, S. Desprez, M. Descamps, Crystallization and glass properties of pentitols, J. Therm. Anal. Calorim. 73 (2003) 577–586.
[150] H. Zhang, S.V. Nedea, C.C. Rindt, Review and in silico characterization of sugar alcohols as season heat storage materials, in: 13th International Conference on Energy Storage (Greenstock 2015), May 19-21, Beijing, China, 2015.
[151] H. Zhang, M. Duquesne, A. Godin, S. Niedermaier, E. Palomo del Barrio, S.V. Nedea, C.C. Rindt, Experimental and in silico characterization of xylitol as seasonal heat storage material, Fluid Phase Equilib. 436 (2017) 55–68.
[152] W. Guex, H. Klaeui, H. Pauling, F. Voirol, Reusable Heat Devices Containing Xylitol as the Heat-Storage Material, Technical Report, 1981.
[153] F. Roget, Définition, Modélisation et Validation Expérimentale d'Une Capacité de Stockage Thermique par Chaleur Latente Adaptée à une Centrale Thermodynamique Solaire à Basse Température (Ph.D. thesis), Toulon, 2012.
[154] S.N. Gunasekara, J.N. Chiu, V. Martin, P. Hedström, The experimental phase diagram study of the binary polyols system erythritol-xylitol, Sol. Energy Mater. Sol. Cells 174 (2018) 248–262.
[155] R.A. Talja, Y.H. Roos, Phase and state transition effects on dielectric, mechanical, and thermal properties of polyols, Thermochim. Acta 380 (2001) 109–121.
[156] A. Godin, M. Duquesne, E. Palomo del Barrio, J. Morikawa, Analysis of crystal growth kinetics in undercooled melts by infrared thermography, Quant. InfraRed Thermogr. J. 12 (2015) 237–251.
[157] M. Kubota, E.P. Ona, F. Watanabe, H. Matsuda, H. Hidaka, H. Kakiuchi, Studies on phase change characteristics of binary mixtures of erythritol and MgCl2·6H2O, J. Chem. Eng. Japan 40 (2007) 80–84.
[158] H. Zhang, On Sugar Alcohol Based Heat Storage Materials: A Nanoscale Study and beyond (Ph.D. thesis, Doctoral Dissertation), TU/e Eindhoven University of Technology, Eindhoven, 2017.
[159] X.-F. Shao, J.-C. Lin, H.-R. Teng, S. Yang, L.-W. Fan, J.N. Chiu, Z.-T. Yu, V. Martin, Hydroxyl group functionalized graphene oxide nanosheets as additive for improved erythritol latent heat storage performance: A comprehensive evaluation on the benefits and challenges, Sol. Energy Mater. Sol. Cells 215 (2020) 110658.
[160] N. Beemkumar, A. Karthikeyan, B. Saravanakumar, J. Jayaprabakar, Performance improvement of d-sorbitol pcm-based energy storage system with different fins, Int. J. Ambient Energy 39 (2018) 372–376.
[161] J.-L. Zeng, Y.-H. Chen, L. Shu, L.-P. Yu, L. Zhu, L.-B. Song, Z. Cao, L.-X. Sun, Preparation and thermal properties of exfoliated graphite/erythritol/mannitol eutectic composite as form-stable phase change material for thermal energy storage, Sol. Energy Mater. Sol. Cells 178 (2018) 84–90.
[162] M. Pramothraj, R. Santosh, M. Swaminathan, et al., Study of effect of al and cu microparticles dispersed in d-mannitol pcm for effective solar thermal energy storage, J. Therm. Anal. Calorim. 139 (2020) 895–904.
[163] S. Guo, Q. Liu, J. Zhao, G. Jin, X. Wang, Z. Lang, W. He, Z. Gong, Evaluation and comparison of erythritol-based composites with addition of expanded graphite and carbon nanotubes, Appl. Energy 205 (2017) 703–709.
[164] Q. Zhang, Z. Luo, Q. Guo, G. Wu, Preparation and thermal properties of short carbon fibers/erythritol phase change materials, Energy Convers. Manage. 136 (2017) 220–228.
[165] S. Shen, S. Tan, S. Wu, C. Guo, J. Liang, Q. Yang, G. Xu, J. Deng, The effects of modified carbon nanotubes on the thermal properties of erythritol as phase change materials, Energy Convers. Manage. 157 (2018) 41–48.
[166] M. Vivekananthan, V.A. Amirtham, Characterisation and thermophysical properties of graphene nanoparticles dispersed erythritol pcm for medium temperature thermal energy storage applications, Thermochim. Acta 676 (2019) 94–103.
[167] J. Ji, Y. Wang, X. Zhang, Y. Chen, J.M. Munyalo, S. Liu, Supercooling characteristics of mannitol phase transition system under heterogeneous nucleation, J. Mater. Sci. 55 (2020) 2994–3004.
[168] W. Li, D. Zhang, T. Zhang, T. Wang, D. Ruan, D. Xing, H. Li, Study of solid–solid phase change of (n-CnH2n+1NH3)2MCl4 for thermal energy storage, Thermochim. Acta 326 (1999) 183–186.
[169] H. Feng, X. Liu, S. He, K. Wu, J. Zhang, Studies on solid–solid phase transitions of polyols by infrared spectroscopy, Thermochim. Acta 348 (2000) 175–179.
[170] W. Li, D. Zhang, T. Zhang, T. Wang, D. Ruan, D. Xing, H. Li, Study of solid–solid phase change of (n-cnh2n+1nh3)2mcl4 for thermal energy storage, Thermochim. Acta 326 (1999) 183–186.
[171] J. Font, J. Muntasell, J. Navarro, J. Tamarit, J. Lloveras, Calorimetric study of the mixtures PE/NPG and PG/NPG, Solar Energy Mater. 15 (1987) 299–310.
[172] E. Murrill, L. Breed, Solid—solid phase transitions determined by differential scanning calorimetry: Part i. tetrahedral substances, Thermochim. Acta 1 (1970) 239–246.
[173] H.A. Rose, A. Van Camp, Crystallographic data. 139. 2-amino-2-methyl-1, 3-propanediol, Anal. Chem. 28 (1956) 1790–1791.
[174] P. Lloveras, A. Aznar, M. Barrio, P. Negrier, C. Popescu, A. Planes, L. Mañsa, E. Stern-Taulats, A. Avramenko, N.D. Mathur, X. Moya, J.-L. Tamarit, Colossal barocaloric effects near room temperature in plastic crystals of neopentylglycol, Nature Commun. 10 (2019) 1803.
[175] B. Li, Y. Kawakita, S. Ohira-Kawamura, T. Sugahara, H. Wang, J. Wang, Y. Chen, S.I. Kawaguchi, S. Kawaguchi, K. Ohara, K. Li, D. Yu, R. Mole, T. Hattori, T. Kikuchi, S. Yano, Z. Zhang, Z. Zhang, W. Ren, S. Lin, O. Sakata, K. Nakajima, Z. Zhang, Colossal barocaloric effects in plastic crystals, Nature 567 (2019).
[176] F.B. Li, M. Li, X. Xu, Z.C. Yang, H. Xu, C.K. Jia, K. Li, J. He, B. Li, H. Wang, Understanding colossal barocaloric effects in plastic crystals, Nature Commun. 11 (2020).
[177] R. Shi, D. Chandra, W.-M. Chien, J. Wang, High-throughput thermodynamic computation and experimental study of solid-state phase transitions in organic multicomponent orientationally disordered phase change materials for thermal energy storage, CALPHAD 64 (2019) 66–77.
[178] J. Timmermans, Plastic crystals: A historical review, J. Phys. Chem. Solids 18 (1961) 1–8.
[179] Q. Yan, C. Liang, The thermal storage performance of monobasic, binary and triatomic polyalcohols systems, Sol. Energy 82 (2008) 656–662.
[180] M. Barrio, J. Font, D. López, J. Muntasell, J. Tamarit, P. Negrier, N. Chanh, Y. Haget, Miscibility and molecular interactions in plastic phases: Binary system pentaglycerin/ tris(hydroxymethyl)aminomethane, J. Phys. Chem. Solids 54 (1993) 171–181.
[181] A. Mishra, A. Talekar, D. Chandra, W.-M. Chien, Ternary phase diagram calculations of pentaerythritol–pentaglycerine–neopentylglycol system, Thermochim. Acta 535 (2012) 17–26.
[182] D. Chandra, R. Chellappa, W.-M. Chien, Thermodynamic assessment of binary solid-state thermal storage materials, J. Phys. Chem. Solids 66 (2005) 235–240, Proceedings of the 11th International Conference on High Temperature Materials Chemistry (HTMC-XI).
[183] R. Shi, D. Chandra, A. Mishra, A. Talekar, M. Tirumala, D.J. Nelson, Thermodynamic reassessment of the novel solid-state thermal energy storage materials: Ternary polyalcohol and amine system pentaglycerine-tris(hydroxymethyl)-amino-methane-neopentylglycol (PG-TRIS-NPG), CALPHAD 59 (2017) 61–75.
[184] B. Feng, J. Tu, J.-W. Sun, L.-W. Fan, Y. Zeng, A molecular dynamics study of the effects of crystalline structure transition on the thermal conductivity of pentaerythritol as a solid–solid phase change material, Int. J. Heat Mass Transfer 141 (2019) 789–798.

[185] D. Benson, R. Burrows, J. Webb, Solid state phase transitions in pentaerythritol and related polyhydric alcohols, Solar Energy Mater. 13 (1986) 133–152.
[186] Y. Li, M. Wu, R. Liu, Y. Huang, Cellulose-based solid–solid phase change materials synthesized in ionic liquid, Sol. Energy Mater. Sol. Cells 93 (2009) 1321–1328.
[187] C.R. Raj, S. Suresh, R. Bhavsar, V. Kumar Singh, S. Reddy, Effect of nano-gallium capsules on thermal energy storage characteristics of manganese organometallic SS-PCM, Thermochim. Acta 680 (2019) 178341.
[188] N. Zhang, Y. Jing, Y. Song, Y. Du, Y. Yuan, Thermal properties and crystallization kinetics of pentaglycerine/graphene nanoplatelets composite phase change material for thermal energy storage, Int. J. Energy Res. 44 (2020) 448–459.
[189] K. Venkitaraj, S. Suresh, Experimental study on thermal and chemical stability of pentaerythritol blended with low melting alloy as possible pcm for latent heat storage, Exp. Therm Fluid Sci. 88 (2017) 73–87.
[190] K. Venkitaraj, S. Suresh, B. Praveen, A. Venugopal, S.C. Nair, Pentaerythritol with alumina nano additives for thermal energy storage applications, J. Energy Storage 13 (2017) 359–377.
[191] K. Venkitaraj, S. Suresh, B. Praveen, S.C. Nair, Experimental heat transfer analysis of macro packed neopentylglycol with cuo nano additives for building cooling applications, J. Energy Storage 17 (2018) 1–10.
[192] B. Praveen, S. Suresh, Experimental study on heat transfer performance of neopentyl glycol/cuo composite solid–solid pcm in tes based heat sink, Eng. Sci. Technol. Int. J. 21 (2018) 1086–1094.
[193] A. Mishra, A. Talekar, D. Chandra, W.-M. Chien, Ternary phase diagram calculations of pentaerythritol–pentaglycerine–neopentylglycol system, Thermochim. Acta 535 (2012) 17–26.
[194] A. Serrano, M. Duran, J.-L. Dauvergne, S. Doppiu, E.P. Del Barrio, Tailored transition temperature plastic crystals with enhanced thermal energy storage capacity, Sol. Energy Mater. Sol. Cells 220 (2021) 110848.
[195] M. Barrio, J. Font, J. Muntasell, J. Navarro, J. Tamarit, Applicability for heat storage of binary systems of neopentylglycol, pentaglycerine and pentaerythritol: A comparative analysis, Solar Energy Mater. 18 (1988) 109–115.
[196] M. Barrio, J.T. Font, D.O. López, J. Muntasell, J.L. Tamarit, P. Négrier, Y. Haget, Miscibility in plastic phases: Binary system NPG (neopentylglycol)/AMP (2-amino, 2-methyl-1, 3-propanediol), J. Phys. Chem. Solids 55 (1994) 1295–1302.
[197] D. Chandra, R. Chellappa, W.-M. Chien, Thermodynamic assessment of binary solid-state thermal storage materials, J. Phys. Chem. Solids 66 (2005) 235–240, Proceedings of the 11th International Conference on High Temperature Materials Chemistry (HTMC-XI).
[198] A. Solé, L. Miró, C. Barreneche, I. Martorell, L.F. Cabeza, Review of the t-history method to determine thermophysical properties of phase change materials (pcm), Renew. Sustain. Energy Rev. 26 (2013) 425–436.